



Forward and inverse modelling of eco-evolutionary dynamics



in biological and economic systems

Victor Boussange

Forward and inverse modelling of eco-evolutionary dynamics in biological and economic systems

September 12, 2022

Cover picture: Top: forest in Sorapiss, Dolomites, Italy. Bottom: New York City, USA. @ Luca
Bravo / PhotoSpirit

The document format is based on the *Clean Thesis* style developed by Ricardo Langner.

Contents

1	Introduction	1
2	Eco-evolutionary model on spatial graphs reveals how habitat structure affects phenotypic differentiation	13
2.1	Introduction	15
2.2	Results	17
2.2.1	Eco-evolutionary model on spatial graphs	17
2.2.2	Deterministic approximation of the population dynamics under no selection	19
2.2.3	Effect of graph topology on neutral differentiation under no selection	20
2.2.4	Deterministic approximation of the population dynamics and adaptation under heterogeneous selection	22
2.2.5	Effect of graph topology on adaptive differentiation under heterogeneous selection	24
2.2.6	Effect of habitat assortativity on neutral differentiation under heterogeneous selection	26
2.3	Discussion	29
2.4	Methods	31
2.4.1	Mean field approximation	31
2.4.2	Adaptive dynamics on graphs	32
2.4.3	Numerical simulations	33
2.4.4	Statistics and reproducibility	34
2.A	Supplementary Note	40
2.A.1	Mathematical construction of the model	40
2.A.2	Deterministic approximation	42
2.A.3	Trait-dependent competition	44
2.A.4	Derivation of the habitat assortativity metric r_{Θ} in binary environments	45
2.B	Supplementary Figures	48
2.C	Supplementary Tables	59

3 Discussion	65
3.1 Contributions	65
3.1.1 Advances in the fundamental understanding of biological and economic systems	65

Introduction

” Concepts without precepts are empty, and precepts without concepts are blind.

— Immanuel Kant
Critique of Pure Reason

Biological and economic systems as complex adaptive systems

What are the similarities between biological and economic systems? Both are complex adaptive systems (CAS) [1], which are composed of heterogeneous entities structured at different levels of organizations, that interact in nonlinear ways and experience evolutionary processes. Interaction and evolutionary processes take many different forms and operate at different organizational level [Levin1998] (see Fig. 1.1). Interestingly, the variety of processes involved and their couplings do not necessarily lead to unpredictable, chaotic, or erratic structures and dynamics [Olff2009], but rather induce organised structural properties and behavior [mitchell2009complexity]. In biological systems, those include patterns of species richness, where for instance montane regions are often associated with a disproportionately high number of species [2]. In economic systems, those include the distribution of international income, where some countries have systematically developed much more rapidly than others [acemoglu2001colonial]. A common direction on the research agenda in Biology and Economics is to comprehend the set of interaction and evolutionary processes that determine these emergent properties [3], and how do they do so. In biological systems, the nature of the processes of interaction and evolution is identified, and the current challenge is to comprehend the mechanisms resulting from their couplings. In economic systems, we still do not exactly understand the nature of those processes, and how are they involved.

Ecological and evolutionary processes drive the dynamics of biological systems

In biological systems, interaction processes are generally designated as ecological processes, and involve fluxes of energy and matter across space and time, encompassing the processes of interaction between organisms (biotic interactions) and between

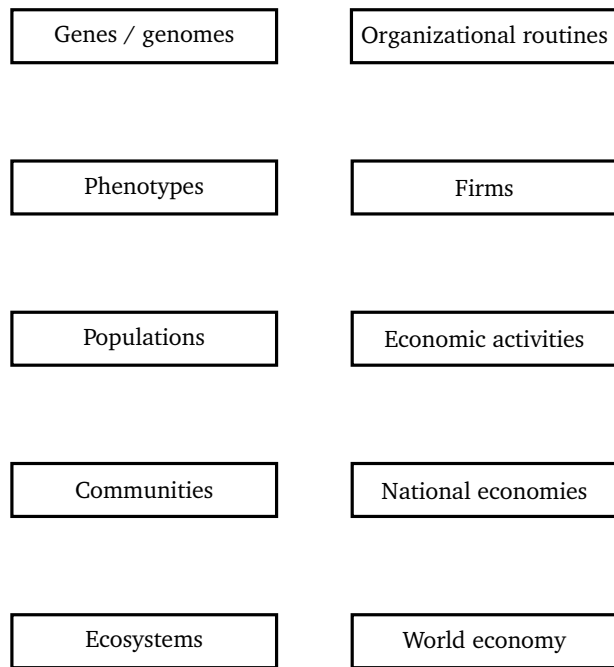


Fig. 1.1: Schematic diagram of proposed organisational levels in biological and economic systems. A is inspired from [Hendry+2016]

organisms and their environment (abiotic interactions), and dispersal processes (movement of individual across space) [4]. Evolutionary processes designate those processes responsible for the change of heritable characteristics (DNA, genes, phenotypes) over successive generations [Hall2013]. The coupling between ecological and evolutionary processes is acknowledged since the very birth of the theory of Evolution, when Darwin realised a link between the different ecological opportunities across the Galápagos islands and the different beak shapes in the finches he found in each island [darwin2004origin], during his voyage on the Beagle. He reasoned that the variations in ecological opportunities lead to a differential in survival for certain phenotypes, which over time resulted in the evolution of different beak shapes. Since then, we know that ecological processes directly affect evolutionary response [Ezard2009]. In the recent years, the idea that not only ecological processes can affect evolutionary response, but also that evolutionary processes could affect ecological processes, has developed [XXX]. Empirical studies have demonstrated that evolution can be rapid and occur on similar time scales as ecology [Hairston2005, 5] and have quantifiable effects on ecological dynamics [Ezard2009], leading to feedbacks between ecological and evolutionary processes, so-called eco-evolutionary feedbacks [Schoener2011, 5]. Eco-evolutionary feedbacks involve situations where an ecological property influences evolutionary change, which then feeds back to an ecological property, or vice versa [Govaert2019a]. Examples are feedbacks

between population density (ecological property) and trait evolution (evolutionary change), which can lead to evolutionary branching through the effect of competition [Doebeli1999]. Eco-evolutionary feedbacks are also involved in adaptation mechanisms [Doebeli1999], where species disperse and phenotypic variations allow to adapt to local environments [XXX]. Those feedbacks may greatly influence the mechanisms driving the dynamics of ecosystems [6], but our understanding of their nature and effect is limited [Lion2022]. In particular, eco-evolutionary feedbacks are expected to play a critical role in the evolution of the biosphere in the coming decades [7], as ecosystems are being rapidly affected by anthropogenic pressure and with climate change [8, 9]. In order to mitigate the consequences of human development, it is of utmost urgency to better understand eco-evolutionary feedbacks [7], and develop mechanistic models embedding this knowledge [6]. This will in turn provide more reliable forecasts of ecosystem states [Clark2001], to help designing adequate management of ecosystem services [6].

Drivers of economic change

The processes that determine economic change is controversial in economics [Nelson2014]. To explain economic development, mainstream economic theory [10.1093/cje/bet027] assumes that economic systems are in equilibrium, in the sense that the demand and supply of goods and services are balanced on all relevant markets. Firms are rational in maximizing profits by adapting to demand and supply, and the observed economic change is driven by exogenous forces, such as technological change [Romer1986]. Evolutionary economics, promoted by the seminal work of Ref. [Nelson2014], criticizes this view and seeks to explain economic change by focusing on endogenous forces. Evolutionary economics suggests that interactions between firms and economic activities, and evolutionary processes acting upon them, are major processes contributing to economic change [Hodgson2019]. For instance, firms or economic activities may interact positively or negatively [Wernerfelt1989, Pistorius2007Ozman2009, Saavedra2009a, Cohendet2018, Menon2015], spread across space [RogersEverettM2003DoI, Zahra2000], and adapt [Cordes2006] or transform into new economic institutions [Freeman2002, Hodgson2004, Aldrich2008], affecting economic development at the regional and national scale. Because these processes are analogous to eco-evolutionary processes driving the dynamics of biological systems, a number of modelling approaches have borrowed concepts and methods from biology in the last decades, aiming at better understanding the processes underlying emergent properties in economic systems [Tacchella2018, Saavedra2009a, Scholl2020, Zhang2018, Modis1997, Saavedra2014, Farmer1999, Michalakelis2011, Marasco2016, Gatabazi2019,

Cauwels2016, **Applegate2021**, **Suweis2015**]. For instance, [Saavedra2009a] has successfully used a model of mutualistic interaction to explain structural patterns in industrial cooperation. Also, [Scholl2020] uses the concepts of foodwebs and density dependence to explain market malfunctions and excess volatility in financial markets. However, those studies did not seek to understand how these processes may affect economic development. Recent modelling approaches developed in evolutionary biology may help to disentangle whether eco-evolutionary processes could explain differences in economic development across countries.

Forward modelling of eco-evolutionary processes

The complex interplay between ecological and evolutionary processes, acting at different scales of time and space and organization, can hardly be studied with experimental approaches [Hagen2022, 10]. As such, a deductive approach, relying on forward modelling, has traditionally been put forward to advance our understanding of the mechanisms underlying [Brummitt2020]. Along this approach, hypotheses about causal processes are embedded in a model, which forward integration generates emergent properties. Such emergent behavior may be seen as predictions from the consideration of the causal processes [May2004]. The role of the modeller is to point at the mechanisms by which the properties emerge, disentangling the underlying interplay between the processes. In the early 1930s to 1940s, by formulating tractable mathematical models implementing the processes of reproduction, dispersal and mutations, the work of Fisher, Wright and Haldane has greatly contributed to the modern synthesis of evolutionary biology [huxley1942evolution], generally accepted as the basis of our current understanding of evolutionary dynamics. The mechanistic models commonly take the form of differential equations (DE), and express how the processes under investigation affect the rate of change of the population characteristics, such as the proportion of a given allele. However, the requirement of tractable mathematical models (DEs that yield analytical solutions) has involved strong assumptions on the processes investigated, that are poorly representative of the complexity of eco-evolutionary feedbacks in nature [Govaert2019a]. In particular, ecological scenarios have been strongly simplified, and did not take into account how evolution could affect population dynamics [Lion2022]. As such, traditional mathematical models have omitted eco-evolutionary feedbacks and density dependence.

With the increase in computational capacity, novel modelling approaches relying on individual based models (IBMs) have appeared [deangelis2005individual]. IBMs allow to capture processes acting at the individual level, requiring less simplifying assumptions than traditional mathematical models [deangelis2005individual].

Capturing more realistic scenarios by allowing the forward integration of complex hypothesis, the lack of analytical tractability of IBMs may nonetheless occult the mechanisms underlying emergent properties [**May2004**, 11]. The recent development of mathematical techniques, such moment closure approximations [**law1999moment**, **Gandhi2000**, 12, 11], adaptive dynamics theory [**Metz1995**], and probability theory [13], are generating novel pathways by filling the gap between IBMs and mathematical models. Analogous to renormalisation group analysis developed in quantum and statistical physics [**Sayama**], they form a toolbox to rigorously derive how emergent properties are influenced by processes operating at different organizational levels. As such, they allow an analytical underpinning to IBM simulations, and can generate a general understanding of the key mechanisms at stake [11].

The combination of numerical simulations and, e.g., adaptive dynamics theory, has successfully shed new lights on on the emergence of evolutionary branching under frequency-dependent selection [14, 15]. An other example is the work of [**Debarre2013a**, 16, 17], that has provided new insights on the effect of habitat heterogeneity on population dynamics. However, our current understanding of eco-evolutionary feedbacks omits potentially significant factors, such as the structuration of populations over complex spatial structures [**XX**] and highly dimensional phenotypic space [**XXX**].

The consideration of such details is important to advance our understanding, but raises challenging methodological issues. In particular, complex models may hinder the fundamental mechanisms underlying the emergence of a pattern. Also, the consideration of multiple traits leads to an increase in the dimensionality of the associated DE problem, which in turn leads to an exponential increase in computational cost [**XXX**]. In order to better understand eco-evolutionary feedbacks, we need to investigate more realistic scenarios, which will, in turn, require the development of novel numerical methods that can cope with the extra computational cost.

Inverse modelling

Diametrically opposed to forward modelling, inverse modelling consists in using observation data to infer causal processes [18]. Inverse modelling has recently seen an increased attention, thanks to the increased computational power and availability of datasets [**Csillary2010**]. It involves the use of inference methods to estimate model parameters, such as bayesian or maximum likelihood inference methods [19]. Those methods proceed by defining a distance between the model simulation and the observation data, which relates to the probability of the parameters given the

model and the data [19]. The most likely parameters are associated with the minimum distance, obtained using ad-hoc algorithms. Provided that they are inferred together with uncertainties, parameters can be interpreted to better understand the strengths and effects of the embedded processes [10]. For instance, [20, 21] infers and analyse the parameters of population dynamic models to understand processes involved in ecosystem functions. Because the parameter estimation problem is equivalent to finding the maximum probability of the model given the observation data, inference methods can also be used to discriminate between candidate mechanisms embedded in alternative models [22, 23]. For instance, [Skeels2022] shows that temperature-dependent evolutionary speed is the most likely mechanism to explain variations in biodiversity patterns, using inference methods to discriminate between alternative dynamic models embedding different hypotheses. Nonetheless, the use of inverse modelling in evolutionary biology has been limited because of a number of issues, some of which specifically relating to eco-evolutionary models. Central to these issues are the high computational cost of the forward integration of eco-evolutionary models [24], the large number of parameters involved [25], and their strong nonlinearities[26, 27, 28]. Advances in the field of artificial intelligence could circumvent these issues.

Machine learning to leverage forward and inverse modelling

In the recent years, the field of artificial intelligence (AI) has made enormous progresses in computer vision [XXX] and natural language processing [XXX]. At the backbone of this success are key computational techniques that could leverage the forward and inverse modelling of CAS. Computer vision and natural language processing rely on deep learning methods, that allow neural networks to learn abstract representation of mechanisms from large datasets [29]. These abstractions are hardly interpretable by humans [XXX], and their prediction ability is limited by the information contained in the training datasets. As such, neural networks cannot be used *per se* to gain scientific insights and extrapolate beyond observed trends [30, 6]. Nevertheless, their traditional applications and associated methods have been successfully derived in other scientific fields for this purpose [Rolnick2023, 31, 32, 33].

Neural networks have been used in forward modelling, to reduce the cost of the forward integration of climate models, by learning more efficient representations of physical mechanisms [XXX]. They have also been used to approximate the solution of partial differential equations (PDEs) [34], with the major advantage of approximating high dimensional problems at a lower computational cost than traditional methods. Underlying the training of neural network is the technique of

backpropagation [XXX]. This technique can be generalised to any scientific model against data [35], with the potential to leverage inverse modelling techniques. As such, the derivation of AI techniques to investigate causal processes in CAS offers unique opportunities [**Frank2022**].

Programming languages

Combining ML techniques with scientific models requires computational environments that allow to easily develop scientific models, ensure simulation performance, and provide composability between ML and other scientific libraries [35]. Unfortunately, performance and composability are features that are poorly represented in mainstream programming languages used by the scientific community, such as Python, Matlab or R. Those languages are naturally attractive because they are dynamically typed [XX], allowing convenient development iterations. Nonetheless, prototypes written in Python, Matlab or R need to be rewritten in low level, compiled languages such as C, C++ or Fortran for speed and predictable mapping to hardware [**Perkel2019**, **Bezanson2017**]. This conversion requires significant involvement, leading to a problem commonly designated as the "two language problem" [**Bezanson2017**]. In order to circumvent issues of performance, most libraries in Python, Matlab or R rely on bindings with low level languages. For instance, the most used deep learning libraries in Python, TensorFlow and PyTorch, are internally written in C. However, bindings with low level languages come with major negative externalities, such as restricting the understandability of their internals to computer scientists – prohibiting potential development contributions from the scientific community –, and preventing the composability of libraries [XXX].

Julia is a programming language that was launched in 2012 to address the issue of the two-language problem [**Bezanson2017**, **Bezanson2018**]. Julia was built over a type-specializing, just-in-time compiler, which makes it easy to generate highly performant programs, while preserving the essential features of Python, Matlab or R, such as dynamic typing and automatic memory management. Importantly, it relies on multiple dispatch, which allows to generate highly generic code with good performance. This permits to write libraries in pure Julia, guaranteeing productivity and composability. As such, the internals of any Julia library can be understood by non computer-scientists, who can further use his expertise to participate to its development. Many Julia libraries benefit from a high number of contributions of independent users (see, e.g., github.com/DifferentialEquations.jl). Multiple dispatch also allows to automatically generate the gradient of any Julia program without any modification [**ForwardDiff.jl**, **Zygote.jl**]. This means that any scientific library in Julia, such as differential equation solvers, can be combined with deep learning tools,

with unique opportunities for forward and inverse modelling problems [Frank2022]. As such, Julia allows to prototype a program which is readily generic and can directly be shared to the research community. Further, by granting the composability of libraries, it allows to blend ML techniques with scientific models. This makes Julia a promising computational environment to accelerate research in CAS.

Thesis outline

In summary, while it is increasingly acknowledged that feedbacks between ecological and evolutionary processes play an important role in the dynamics of biological systems [5, 6], our understanding of the mechanisms in which they are involved has been limited to simplified scenarios. Further, while analogous processes have been suggested to influence the dynamics of economic systems [Hodgson2019], a quantification of their effect is missing. Under increasing anthropogenic pressure, these research directions become essential [6], but raise challenging methodological issues. Here, I present novel forward and inverse modelling approaches to advance our understanding of eco-evolutionary dynamics in biological and economic systems, and utilise them to shed light on the underlying processes and resulting mechanisms.

In Chapter 2, I investigate how eco-evolutionary processes, in combination with complex habitat spatial structures, influence the trait distribution of biological populations. I proceed using a forward modelling approach, building a stochastic eco-evolutionary IBM where individuals are structured over a spatial graph, and experience the fundamental processes of reproduction, competition, mutation and migration. I seek to understand how those microscopic forces result in trait differentiation at the population level. I derive DE approximations of the IBM that, together with extensive numerical simulations, provide analytical insights into how the graph properties affect the population size and trait differentiation. In particular, I show that three main graph properties, measuring landscape connectivity, heterogeneity in connectivity, and habitat spatial auto-correlation, shape the trait differentiation of the biological population. These results establish mechanistic links between landscape features and the eco-evolutionary dynamics of biological populations.

In ??, I develop an inverse modelling method to estimate the parameters of highly nonlinear population dynamic models. The method is based on a machine learning framework and involves AI techniques together with a novel learning strategy. This learning strategy consists in training the model against mini-batches of data with short time horizon, which I analytically show to regularize the learning problem. I implement the ML framework in the Julia library `MiniBatchInference.jl`, and demonstrate through numerical experiments that it can efficiently estimate model parameters and provide statistical evidences for causal processes from noisy,

incomplete and independent time series. Altogether, the proposed ML framework is a workhorse for inverse modelling and can elucidate mechanistic pathways in biological and economic systems.

In ??, I quantify the effect of eco-evolutionary processes on the dynamics of economic systems. I employ the ML framework developed in ?? to investigate how alternative eco-evolutionary population dynamic models can explain the dynamics of economic activities in the richest 100 countries, relying on 59 year of economic data. The models embed the processes of ecological interactions between economic activities, spatial transfers, and economic activity transformations, which support is compared to a simple logistic growth model, taken as a null model. I find strong statistical evidence for positive interactions between national economic activities, and spatial transfers across countries. To my knowledge, this is the first study that provides quantitative evidences that similar processes may influence the dynamics of biological and economic systems.

In ??, I extend two recent methods to solve high dimensional PDEs, in order to handle non-local nonlinear terms. The first method relies on Picard iterations, while the second is based on machine learning and involves neural networks to approximate PDE solutions. The numerical difficulties arising due to the non-local term are avoided by using a plain vanilla Monte Carlo integration. I implement the methods in the Julia library **HighDimPDE.jl**, and evaluate their performance on high dimensional PDE models arising in physics and biology, including population dynamic eco-evolutionary models. For all models, the methods yield good results with short run times, offering the possibility to include more realism in future eco-evolutionary models.

References

- [1] S. A. Levin. “Complex adaptive systems: Exploring the known, the unknown and the unknowable”. In: *Bulletin of the American Mathematical Society* 40.01 (2002), pp. 3–20. DOI: 10.1090/S0273-0979-02-00965-5.
- [2] C. Rahbek et al. “Humboldt’s enigma: What causes global patterns of mountain biodiversity?” In: *Science* 365.6458 (2019), pp. 1108–1113. DOI: 10.1126/science.aax0149.
- [3] J. M. Nordbotten et al. “Ecological and evolutionary dynamics of interconnectedness and modularity”. In: *Proc. Natl. Acad. Sci. USA* 115.4 (2018), pp. 750–755. DOI: 10.1073/pnas.1716078115.
- [4] M. Vellend. “Conceptual Synthesis in Community Ecology”. In: *The Quarterly Review of Biology* 85.2 (2010), pp. 183–206. DOI: 10.1086/652373.
- [5] F. Pelletier, D. Garant, and A. Hendry. “Eco-evolutionary dynamics”. eng. In: *Philosophical Transactions of the Royal Society of London. Series B, Biological Sciences* 364.1523 (2009), pp. 1483–1489. DOI: 10.1098/rstb.2009.0027.
- [6] M. C. Urban et al. “Improving the forecast for biodiversity under climate change”. In: *Science* 353.6304 (2016). DOI: 10.1126/science.aad8466.
- [7] J. Norberg et al. “Eco-evolutionary responses of biodiversity to climate change”. In: *Nature Climate Change* 2.10 (2012), pp. 747–751. DOI: 10.1038/nclimate1588.
- [8] E. C. Ellis. “Anthropogenic transformation of the terrestrial biosphere”. In: *Philosophical Transactions of the Royal Society A: Mathematical, Physical and Engineering Sciences* 369.1938 (2011), pp. 1010–1035. DOI: 10.1098/rsta.2010.0331.
- [9] G. Midgley and L. Hannah. “Extinction Risk from Climate Change”. In: *Biodiversity and Climate Change*. Yale University Press, 2019, pp. 294–296. DOI: 10.2307/j.ctv8jnzw1.37.
- [10] M. Pontarp, Å. Bränström, and O. L. Petchey. “Inferring community assembly processes from macroscopic patterns using dynamic eco-evolutionary models and Approximate Bayesian Computation (ABC)”. In: *Methods in Ecology and Evolution* 10.4 (2019). Ed. by T. Poisot, pp. 450–460. DOI: 10.1111/2041-210X.13129.
- [11] S. Lion. “Moment equations in spatial evolutionary ecology”. In: *Journal of Theoretical Biology* 405 (2016), pp. 46–57. DOI: 10.1016/j.jtbi.2015.10.014.

- [12] J. M. Nordbotten et al. “The dynamics of trait variance in multi-species communities”. In: *R. Soc. Open Sci.* 7.8 (2020), Article No. 200321, 20 pp. DOI: [10.1098/rsos.200321](https://doi.org/10.1098/rsos.200321).
- [13] N. Champagnat, R. Ferrière, and S. Méléard. “Unifying evolutionary dynamics: From individual stochastic processes to macroscopic models”. In: *Theoretical Population Biology* 69.3 (2006), pp. 297–321. DOI: [10.1016/j.tpb.2005.10.004](https://doi.org/10.1016/j.tpb.2005.10.004).
- [14] U. Dieckmann and M. Doebeli. “On the origin of species by sympatric speciation”. In: *Nature* 400.6742 (1999), pp. 354–357. DOI: [10.1038/22521](https://doi.org/10.1038/22521).
- [15] M. Doebeli and U. Dieckmann. “Speciation along environmental gradients”. In: *Nature* 421.6920 (2003), pp. 259–264. DOI: [10.1038/nature01274](https://doi.org/10.1038/nature01274).
- [16] G. Meszéna, I. Czibula, and S. Geritz. “Adaptive Dynamics in a 2-Patch Environment: A Toy Model for Allopatric and Parapatric Speciation”. In: *Journal of Biological Systems* 05.02 (1997), pp. 265–284. DOI: [10.1142/S0218339097000175](https://doi.org/10.1142/S0218339097000175).
- [17] S. Mirrahimi and S. Gandon. “Evolution of specialization in heterogeneous environments: equilibrium between selection, mutation and migration”. In: *Genetics* 214.2 (2020), pp. 479–491. DOI: [10.1534/genetics.119.302868](https://doi.org/10.1534/genetics.119.302868).
- [18] C. Peng et al. “Integrating models with data in ecology and palaeoecology: advances towards a model-data fusion approach”. In: *Ecology Letters* 14.5 (2011), pp. 522–536. DOI: [10.1111/j.1461-0248.2011.01603.x](https://doi.org/10.1111/j.1461-0248.2011.01603.x).
- [19] M. Schartau et al. “Reviews and syntheses: parameter identification in marine planktonic ecosystem modelling”. In: *Biogeosciences* 14.6 (2017), pp. 1647–1701. DOI: [10.5194/bg-14-1647-2017](https://doi.org/10.5194/bg-14-1647-2017).
- [20] S. I. Higgins, S. Scheiter, and M. Sankaran. “The stability of African savannas: insights from the indirect estimation of the parameters of a dynamic model”. In: *Ecology* 91.6 (2010), pp. 1682–1692. DOI: [10.1890/08-1368.1](https://doi.org/10.1890/08-1368.1).
- [21] A. Curtsdotter et al. “Ecosystem function in predator–prey food webs—confronting dynamic models with empirical data”. In: *Journal of Animal Ecology* 88.2 (2019). Ed. by D. Stouffer, pp. 196–210. DOI: [10.1111/1365-2656.12892](https://doi.org/10.1111/1365-2656.12892).
- [22] D. R. A. Kenneth P. Burnham and Model. *Model Selection and Multimodel Inference*. Ed. by K. P. Burnham and D. R. Anderson. New York, NY: Springer New York, 2002. DOI: [10.1007/b97636](https://doi.org/10.1007/b97636).
- [23] J. B. Johnson and K. S. Omland. “Model selection in ecology and evolution”. In: *Trends in Ecology & Evolution* 19.2 (2004), pp. 101–108. DOI: [10.1016/j.tree.2003.10.013](https://doi.org/10.1016/j.tree.2003.10.013).

- [24] R. A. Fisher et al. “Vegetation demographics in Earth System Models: A review of progress and priorities”. In: *Global Change Biology* 24.1 (2018), pp. 35–54. DOI: 10.1111/gcb.13910.
- [25] I. L. Boyd. “The Art of Ecological Modeling”. In: *Science* 337.6092 (2012), pp. 306–307. DOI: 10.1126/science.1225049.
- [26] A. Hastings et al. “Chaos in Ecology: Is Mother Nature a Strange Attractor?” In: *Annual Review of Ecology and Systematics* 24.1 (1993), pp. 1–33. DOI: 10.1146/annurev.es.24.110193.000245.
- [27] J. Huisman and F. J. Weissing. “Biodiversity of plankton by species oscillations and chaos”. In: *Nature* 402.6760 (1999), pp. 407–410. DOI: 10.1038/46540.
- [28] E. Benincà et al. “Chaos in a long-term experiment with a plankton community”. In: *Nature* 451.7180 (2008), pp. 822–825. DOI: 10.1038/nature06512.
- [29] Y. LeCun, Y. Bengio, and G. Hinton. “Deep learning”. In: *Nature* 521.7553 (2015), pp. 436–444. DOI: 10.1038/nature14539.
- [30] A. D. Barnosky et al. “Approaching a state shift in Earth’s biosphere”. In: *Nature* 486.7401 (2012), pp. 52–58. DOI: 10.1038/nature11018. arXiv: 9605103 [cs].
- [31] K. Kashinath et al. “Physics-informed machine learning: Case studies for weather and climate modelling”. In: *Philosophical Transactions of the Royal Society A: Mathematical, Physical and Engineering Sciences* 379.2194 (2021). DOI: 10.1098/rsta.2020.0093.
- [32] T. Schneider et al. “Earth System Modeling 2.0: A Blueprint for Models That Learn From Observations and Targeted High-Resolution Simulations”. In: *Geophysical Research Letters* 44.24 (2017), pp. 12,396–12,417. DOI: 10.1002/2017GL076101. arXiv: 1709.00037.
- [33] A. Yazdani et al. “Systems biology informed deep learning for inferring parameters and hidden dynamics”. In: *PLOS Computational Biology* 16.11 (2020). Ed. by V. Hatzimanikatis, e1007575. DOI: 10.1371/journal.pcbi.1007575.
- [34] J. Sirignano and K. Spiliopoulos. “DGM: A deep learning algorithm for solving partial differential equations”. In: *J. Comput. Phys.* 375 (2018), pp. 1339–1364.
- [35] C. Rackauckas et al. “Universal Differential Equations for Scientific Machine Learning”. In: *arXiv:2001.04385v3* (2020), 18 pages.

Eco-evolutionary model on spatial graphs reveals how habitat structure affects phenotypic differentiation

by Victor Boussange^{1,2} and Loïc Pellissier^{1,2}

¹ Swiss Federal Research Institute WSL, CH-8903 Birmensdorf, Switzerland

² Landscape Ecology, Institute of Terrestrial Ecosystems, Department of Environmental System Science, ETH Zürich, CH-8092 Zürich, Switzerland

Published in Communications Biology (2022)

doi:10.1038/s42003-022-03595-3

Differentiation mechanisms are influenced by the properties of the landscape over which individuals interact, disperse and evolve. Here, we investigate how habitat connectivity and habitat heterogeneity affect phenotypic differentiation by formulating a stochastic eco-evolutionary model where individuals are structured over a spatial graph. We combine analytical insights into the eco-evolutionary dynamics with numerical simulations to understand how the graph topology and the spatial distribution of habitat types affect differentiation. We show that not only low connectivity but also heterogeneity in connectivity promotes neutral differentiation, due to increased competition in highly connected vertices. Habitat assortativity, a measure of habitat spatial auto-correlation in graphs, additionally drives differentiation under habitat-dependent selection. While assortative graphs systematically amplify adaptive differentiation, they can foster or depress neutral differentiation depending on the migration regime. By formalising the eco-evolutionary and spatial dynamics of biological populations on graphs, our study establishes fundamental links between landscape features and phenotypic differentiation.

2.1 Introduction

Biodiversity results from differentiation processes influenced by the features of the landscape over which populations are distributed [1]. The documentation of high levels of species diversity in mountain regions and riverine systems suggests that complex connectivity patterns and habitat heterogeneity foster differentiation [2, 3, 4, 5]. However, hypotheses formulated based on empirical evidence should be complemented by mechanistic models to crystallise a causal understanding between processes and patterns [6]. While the number of simulation studies is growing steadily [7], such studies often lack a mathematical formalism to facilitate the interpretation of the model outcomes by providing an analytical underpinning to the simulation results [8].

Phenotypic differentiation processes emerge as a result of mutation, selection and migration and can be classified as neutral or adaptive [9]. Neutral differentiation is initiated by the stochastic drift of local phenotypes when spatial isolation and limited dispersal create barriers to gene flow, allowing distinct phenotypes to emerge in spatially structured populations [10]. In contrast, adaptive differentiation results from heterogeneous selection, which promotes distinct, locally well-adapted phenotypes in populations occupying patches with different habitat conditions [11]. The evolution of neutral phenotypes and of adaptive phenotypes are not independent, as selective forces can indirectly select for those neutral phenotypes that happen to be linked to the fittest adaptive phenotypes, a mechanism called the “hitchhiking effect” [12]. Moreover, selection can generate barriers to gene flow between populations in heterogeneous habitat landscapes [13, 14], a phenomenon coined “isolation by environment”, which can amplify neutral differentiation. How neutral processes, adaptive processes and their interplay are affected by landscape features is difficult to comprehend without a formalised mechanistic model [15].

Models link patterns to processes [6], and the explicit representation of the landscape within an eco-evolutionary model can lead to a causal understanding of how landscape features shape differentiation. Spatial graphs provide a convenient mathematical representation of landscapes, where vertices represent suitable habitats hosting populations, and edges capture the connectivity between habitats [16]. Under ecological dynamics, metapopulation models have been used to study the role of graph topology in the persistence and stability of metapopulation [17, 18, 19, 20] and community diversity [21, 22, 23]. Evolutionary mechanisms are nevertheless fundamental drivers of diversity, and should therefore be explicitly integrated into models [24]. Evolutionary game theory explores how graph topology impacts the fixation probability and the fixation time of a mutated phenotype [25]. However, the framework does not consider the continuous accumulation of mutations, and is therefore not suited to addressing the emergence of phenotypic differentiation. By combining a metapopulation model with a model of neutral evolution, [26, 27] investigated how graph topology affects neutral diversity. Their approach demonstrated the key role of topological properties in shaping diversity, and its predictions could be matched with empirical data from e.g. river basins [28]. Nonetheless, diversity results from the combination of neutral and adaptive processes developing at the population level. A first principles modelling approach considering spatial graphs, but also building upon the elementary processes of

ecological interactions, reproduction, mutation and migration may therefore be promising to investigate the emergence of diversity.

Stochastic models for structured populations, rooted in the microscopic description of individuals, offer a generic framework for modelling eco-evolutionary dynamics [29, 30]. In particular, these models can capture the interplay between population dynamics, spatial dynamics and phenotypic evolution, while providing a rigorous set-up for analytical investigation. By anchoring this modelling paradigm in a mathematical framework, the work of Champagnat et al. [29] generalises models of population genetics [31] (investigating the evolution of the frequencies of alleles) and quantitative genetics [32, 33, 34] (investigating the evolution of phenotypic traits), which stimulated research into the link between spatial population structure and neutral differentiation. The framework embraces density-dependent selection, which could explain the emergence of phenotypic differentiation from competition processes [11], and how spatial segregation can emerge as a byproduct of these adaptive processes along environmental gradients [35]. Related models have addressed the effects of landscape dynamics and habitat heterogeneity on adaptive differentiation, providing mathematical insights into the dynamics [36, 37, 38, 39, 40, 41]. Because it accounts for finite population size, the baseline model of Champagnat et al. [29] can also capture neutral differentiation dynamics and therefore the coupling between neutral and adaptive processes [42, 43]. Nonetheless, the aforementioned studies were not spatially explicit [42, 43] or they assumed regular spatial structures (regular graphs [36, 37, 38, 41] or continuous space [35, 39, 40]), therefore not addressing the role of the spatial complexity of landscapes. A stochastic individual-based model using spatial graphs as a representation of the landscape could help formalise fundamental links between landscape features and phenotypic differentiation.

A key challenge is to understand how individual dynamics result in the emergence of differentiation in complex landscapes [44]. Here, we investigate how complex connectivity patterns and habitat heterogeneity affect both neutral and adaptive phenotypic differentiation by constructing an individual-based model (IBM) that accounts for eco-evolutionary dynamics on spatial graphs. The individuals disperse between habitat patches and possess co-evolving neutral and adaptive traits. The finite size of local populations generates neutral differentiation by inducing a stochastic drift in the neutral trait evolution, while heterogeneous selection gives rise to adaptive differentiation. Macroscopic properties of the model are analytically tractable, and we obtain a deterministic approximation of population size and adaptive trait dynamics which connects the emerging patterns to the graph properties that generate them. However, neutral differentiation is stochastic by nature, which complicates its analytical underpinning. We therefore rely on numerical simulations of the IBM to measure the effect of graph topology on neutral differentiation. In the case where heterogeneous selection is absent, we investigate how graph topology affects neutral differentiation. In the case of heterogeneous selection, we investigate how the graph topology, in combination with the spatial distribution of habitat types, affects levels of (i) adaptive and (ii) neutral differentiation. By combining analytical methods with numerical simulations, we expect to identify graph properties that determine the level of differentiation. Overall, our study establishes causal links between landscape properties and population differentiation and contributes to a fundamental understanding of how landscape features promote biodiversity.

2.2 Results

2.2.1 Eco-evolutionary model on spatial graphs

We establish an individual-based model (IBM) where individuals are structured over a trait space and a graph representing a landscape. For the sake of simplicity, we consider the case of asexual reproduction and haploid genetics [29]. Individuals die, reproduce, mutate and migrate in a stochastic fashion, which together results in macroscopic properties. The formulation of the stochastic IBM allows an analytical description of the dynamics at the population level, which links emergent properties to the elementary processes that generate them.

The trait space $\mathcal{X} \subseteq \mathbb{R}^d$ is continuous and can be split into a neutral trait space \mathcal{U} and an adaptive trait space \mathcal{S} . We refer to neutral traits $u \in \mathcal{U}$ as traits that are not under selection, in contrast to adaptive traits $s \in \mathcal{S}$, which experience selection. The graph denoted by G is composed of a set of vertices $\{v_1, v_2, \dots, v_M\}$ that correspond to habitat patches (suitable geographical areas), and a set of edges that constrain the movement of individuals between the habitat patches. We use the original measure of genetic differentiation for quantitative traits Q_{ST} (standing for Q -statistics) in the case of haploid populations [45, 46]. We denote the neutral trait value of the k -th individual on v_i as $u_k^{(i)}$, the number of individuals on v_i as $N^{(i)}$, the mean neutral trait on v_i as $\bar{u}^{(i)}$, and the mean neutral trait in the metapopulation as \bar{u} . It follows that we quantify neutral differentiation $Q_{ST,u}$ as

$$Q_{ST,u} = \sigma_{B,u}^2 / (\sigma_{B,u}^2 + \sigma_{W,u}^2) \quad (2.1)$$

where $\sigma_{B,u}^2 = \mathbb{E} \left[\frac{1}{M} \sum_i (\bar{u}^{(i)} - \bar{u})^2 \right]$ denotes the expected neutral trait variance between the vertices and $\sigma_{W,u}^2 = \frac{1}{M} \sum_i^M \mathbb{E} \left[\frac{1}{N^{(i)}} \sum_k (u_k^{(i)} - \bar{u}^{(i)})^2 \right]$ denotes the average expected neutral trait variance within vertices. We similarly quantify adaptive differentiation $Q_{ST,s}$.

Following the Gillespie update rule [47], individuals with trait $x_k \in \mathcal{X}$ on vertex v_i are randomly selected to give birth at rate $b^{(i)}(x_k)$ and die at rate $d(N^{(i)}) = N^{(i)}/K$, where K is the local carrying capacity. The definition of d therefore captures competition, which is proportional to the number of individuals on a vertex and does not depend on the individuals' traits (we relax this assumption later on). The offspring resulting from a birth event inherits the parental traits, which can independently be affected by mutations with probability μ . A mutated trait differs from the parental trait by a random change that follows a normal distribution with variance σ_μ^2 (corresponding to the continuum of alleles model [48]). The offspring can further migrate to neighbouring vertices by executing a simple random walk on G with probability m . A schematic overview of the two different settings considered is provided in Fig. 2.1. Under the setting with no selection, individuals are only characterised by neutral traits so that $\mathcal{X} = \mathcal{U}$. For individuals on a vertex with trait $x_k \equiv u_k$ we define $b^{(i)}(x_k) \equiv b$, so that the birth rate is constant. This ensures that neutral traits do not provide any selective advantage. Under the setting with heterogeneous selection, each vertex of the graph v_i is labelled by a habitat type with environmental condition Θ_i that

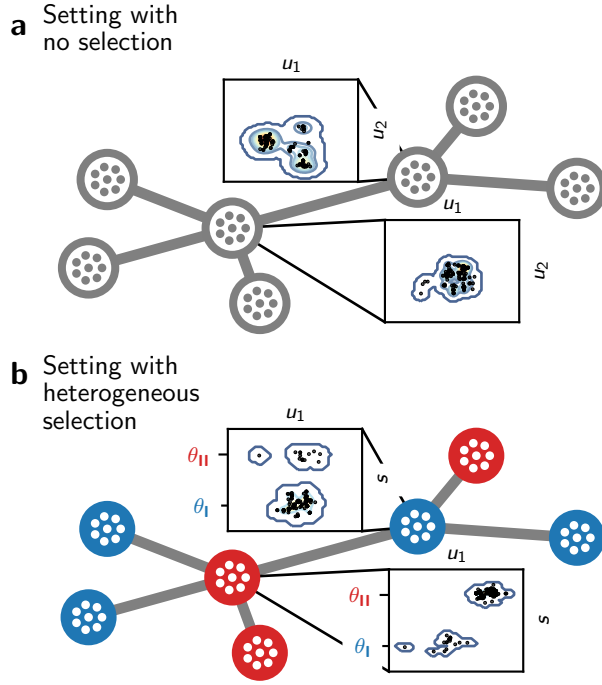


Fig. 2.1: Graphical representation of the structure of individuals in the eco-evolutionary model. (a) Setting with no selection, where individuals are characterised by a set of neutral traits $u \in \mathcal{U}$. The scatter plots represent a projection of the first two components of u for the individuals present on the designated vertices at time $t = 1000$, obtained from one simulation of the IBM. (b) Setting with heterogeneous selection. In this setting, individuals are additionally characterised by adaptive traits $s \in \mathcal{S}$. Blue vertices favour the optimal adaptive trait value θ_\bullet , while red vertices favour θ_\circ . The scatter plots represent a projection of the first component of u and s for the individuals present on the designated vertices at time $t = 1000$, obtained from one simulation. The majority of individuals are locally well-adapted and have an adaptive trait close to the optimal value, but some maladaptive individuals originating from neighbouring vertices are also present. $m = 0.05$.

specifies the optimal adaptive trait value on v_i . It follows that, for individuals with traits $x_k = (u_k, s_k) \in \mathcal{U} \times \mathcal{S}$ on v_i , we define

$$b^{(i)}(x_k) \equiv b^{(i)}(s_k) = b(1 - p(s_k - \Theta_i)^2) \quad (2.2)$$

where p is the selection strength [41]. This ensures that the maximum birth rate on v_i is attained for $s_k = \Theta_i$, which results in a differential advantage that acts as an evolutionary stabilising force. In the following we consider two habitat types denoted by \bullet and \circ with symmetric environmental conditions θ_\bullet and θ_\circ , so that $\Theta_i \in \{\theta_\bullet, \theta_\circ\}$ and $\theta_\circ = -\theta_\bullet = \theta$, where θ can be viewed as the habitat heterogeneity [41].

2.2.2 Deterministic approximation of the population dynamics under no selection

The model can be formulated as a measure-valued point process ([30] and Supplementary Note). Under this formalism, we demonstrate in the Supplementary Note how the population size and the trait dynamics show a deterministic behaviour when a stabilising force dampens the stochastic fluctuations. This makes it possible to express the dynamics of the macroscopic properties with deterministic differential equations, connecting emergent patterns to the processes that generate them. In particular, in the setting of no selection, competition stabilises the population size fluctuations, and the dynamics can be considered deterministic and expressed as

$$\partial_t N_t^{(i)} = N_t^{(i)} \left[b(1 - m) - \frac{N_t^{(i)}}{K} \right] + mb \sum_{j \neq i} \frac{a_{i,j}}{d_j} N_t^{(j)} \quad (2.3)$$

where $A = (a_{i,j})_{1 \leq i,j \leq M}$ is the adjacency matrix of the graph G and $D = (d_1, d_2, \dots, d_M)$ is a vector containing the degree of each vertex (number of edges incident to the vertex). The first term on the right-hand side corresponds to logistic growth, which accounts for birth and death events of non-migrating individuals. The second term captures the gains due to migrations, which depend on the graph topology. Assuming that all vertices with the same degree have an equivalent position on the graph, corresponding to a “mean field” approach (see Methods), one can obtain a closed-form solution from Eq. (2.3) (see Eq. (2.12)), which shows that the average population size \bar{N} scales with $\langle \sqrt{k} \rangle^2 / \langle k \rangle$, where $\langle k \rangle$ is the average vertex degree and $\langle \sqrt{k} \rangle$ is the average square-rooted vertex degree. The quantity $\langle \sqrt{k} \rangle^2 / \langle k \rangle$, denoted as h_d , relates to the homogeneity in vertex degree of the graph and can therefore be viewed as a measure negatively associated with heterogeneity in connectivity. Simulations of the IBM illustrate that h_d can explain differences in population size for complex graph topologies with varying migration regimes (Fig. 2.2a for graphs with $M = 7$ vertices and Fig. S1a for $M = 9$). This analytical result is connected to theoretical work on reaction diffusion processes [49] and highlights that irregular graphs (graphs whose vertices do not have the same degree) result in unbalanced migration fluxes that affect the ecological balance between births and deaths. Highly connected vertices present an oversaturated carrying capacity ($N^{(i)} > bK$, see Methods), increasing local competition and lowering total population size compared with regular graphs (Fig. 2.2a). Because populations with small sizes experience more drift ([31] and Fig. S2), this result indicates that graph topology affects neutral differentiation not only through population isolation, but also by affecting population dynamics.

Nonetheless, the stochasticity of the processes at the individual level can propagate to the population level and substantially affect the macroscopic properties. In particular, neutral differentiation emerges from the stochastic fluctuations of the populations’ neutral trait distribution. These fluctuations complicate an analytical underpinning of the dynamics, and in this case simulations of the IBM offer a straightforward approach to evaluate the level of neutral differentiation.

2.2.3 Effect of graph topology on neutral differentiation under no selection

We study a setting with no selection and investigate the effect of the graph topology on neutral differentiation. When migration is limited, individuals' traits are coherent on each vertex but stochastic drift at the population level generates neutral differentiation between the vertices. Migration attenuates neutral differentiation because it has a correlative effect on local trait distributions. Following [26, 21, 22], we expect that the intensity of the correlative effect depends on the average path length of the graph $\langle l \rangle$, defined as the average shortest path between all pairs of vertices [50]. For a constant number of vertices, $\langle l \rangle$ is strictly related to the mean betweenness centrality and quantifies the graph connectivity [50]. High $\langle l \rangle$ implies low connectivity and a greater isolation of populations, and hence we expect that graphs with high $\langle l \rangle$ are associated with high differentiation levels. We consider various graphs with an identical number of vertices and run simulations of the IBM to obtain the neutral differentiation level $Q_{ST,u}$ attained after a time long enough to discard transient dynamics (see Methods). We then interpret the discrepancies in $Q_{ST,u}$ across the simulations by relating them to the underlying graph topologies.

We observe strong differences in $Q_{ST,u}$ across graphs for varying m , and find that $\langle l \rangle$ explains at least 55% of the variation in $Q_{ST,u}$ across all graphs with $M = 7$ vertices for (Fig. 2.2b). Nonetheless, some specific graphs, such as the star graph, present higher levels of $Q_{ST,u}$ than expected by their average path length. To explain this discrepancy, we explore the effect of homogeneity in vertex degree h_d , as we showed in Eq. (2.12) that it decreases population size, which should in turn increase $Q_{ST,u}$ by intensifying stochastic drift. We find that h_d explains 57% of the variation for low m (Fig. 2.2c). However, the fit remains similar after correcting for differences in population size (see Table S1), indicating that irregular graphs structurally amplify the isolation of populations. Unbalanced migration fluxes lead central vertices to host more individuals than allowed by their carrying capacity. This causes increased competition that results in a higher death rate, so that migrants have a lower probability of further spreading their trait. Highly connected vertices therefore behave as bottlenecks, increasing the isolation of peripheral vertices and consequently amplifying $Q_{ST,u}$.

We then evaluate the concurrent effect of $\langle l \rangle$ and h_d on $Q_{ST,u}$ with a multivariate regression model that we fit independently for low and high migration regimes (Fig. 2.2d). The multivariate regression model explains at least 70% of the variation in $Q_{ST,u}$ for the migration regimes considered and for graphs with $M = 7$ vertices (see Table S2 for details). Moreover, we find that $\langle l \rangle$ and h_d have akin contributions to neutral differentiation for low m , but the effect of $\langle l \rangle$ increases for higher migration regimes while the effect of h_d decreases. To ensure that these conclusions can be generalised to larger graphs, we conduct the same analysis on a subset of graphs with $M = 9$ vertices and find congruent results (Fig. S1). In the absence of selection and with competitive interactions, graphs with a high average path length $\langle l \rangle$ and low homogeneity in vertex degree h_d , or similarly graphs with low connectivity and high heterogeneity in connectivity, show high levels of neutral differentiation.

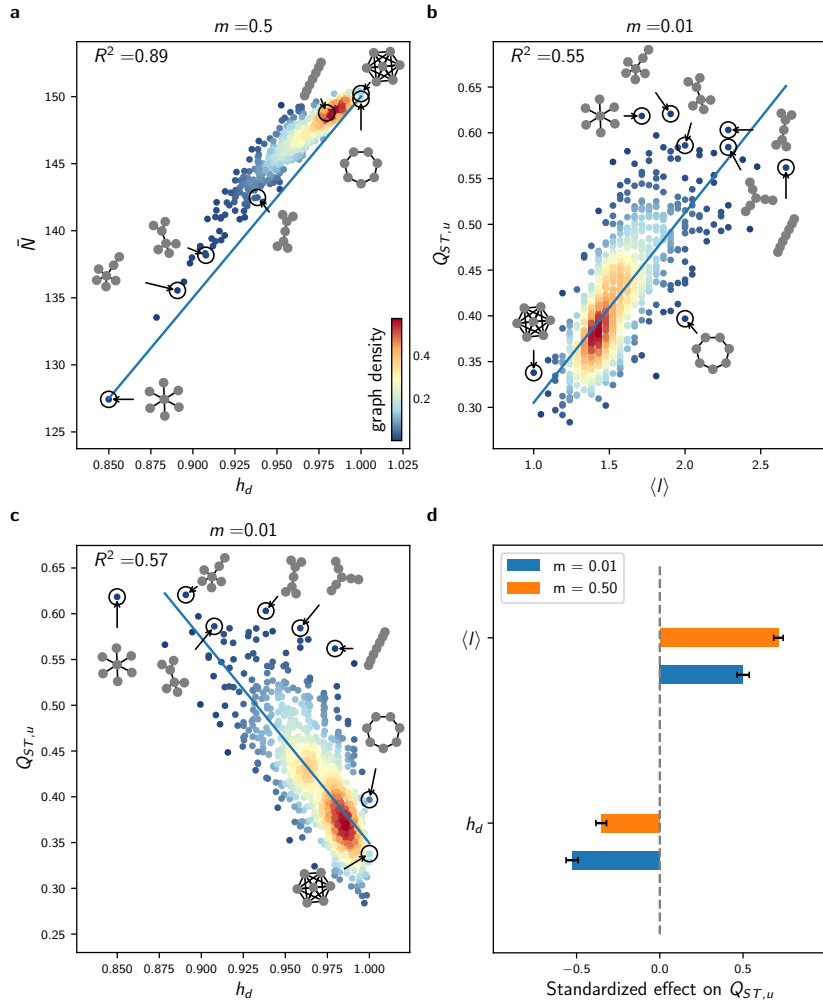


Fig. 2.2: Effect of $\langle l \rangle$ and h_d on average population size \bar{N} and neutral differentiation $Q_{ST,u}$ in the setting with no selection. (a) Response of \bar{N} to homogeneity in degree $h_d = \langle \sqrt{k} \rangle^2 / \langle k \rangle$ for all undirected connected graphs with $M = 7$ vertices and $m = 0.5$. (b) Response of $Q_{ST,u}$ to average path length $\langle l \rangle$ for similar simulations obtained with $m = 0.01$. (c) Response of $Q_{ST,u}$ to homogeneity in degree h_d for the same data. In (a), (b) and (c), each dot represents average results from 5 replicate simulations of the IBM, the colour scale corresponds to the proportion of the graphs with similar x and y axis values (graph density), and the blue line corresponds to a linear fit. (d) Standardized effect of h_d and $\langle l \rangle$ on $Q_{ST,u}$, obtained from multivariate regression models independently fitted on similar data obtained for $m = 0.01$ and $m = 0.5$. The contributions of $\langle l \rangle$ and h_d to $Q_{ST,u}$ are alike for low migration regimes. Error bars show 95% confidence intervals. Analogous results on graphs with $M = 9$ vertices are presented in Fig. S1 and all regression details can be found in Table S2.

2.2.4 Deterministic approximation of the population dynamics and adaptation under heterogeneous selection

We next consider heterogeneous selection and investigate the response of adaptive differentiation to the spatial distribution of habitat types, denoted as the Θ -spatial distribution. Adaptive differentiation emerges from local adaptation, but migration destabilises adaptation as a result of the influx of maladaptive migrants. We expect that higher connectivity between vertices of similar habitat type increases the level of adaptive differentiation, because it increases the proportion of well-adapted migrants. Local adaptation can be investigated by approximating the stochastic dynamics of the trait distribution with a deterministic partial differential equation (PDE). We demonstrate under mean field assumption how the deterministic approximation can be reduced to an equivalent two-habitat model. We analyse the reduced model with the theory of adaptive dynamics [36, 41] and find a critical migration threshold m^* that determines local adaptation. m^* depends on a quantity coined the habitat assortativity r_Θ , and we demonstrate with numerical simulations that r_Θ determines the overall adaptive differentiation level $Q_{ST,s}$ reached at steady state in the deterministic approximation.

Heterogeneous selection, captured by the dependence of the birth rate on Θ_i , generates a stabilising force that dampens the stochastic fluctuations of the adaptive trait distribution. The dynamics of the adaptive trait distribution consequently shows a deterministic behavior and we demonstrate in the Supplementary Note and Figs. S3 and S4 that the number of individuals on v_i with traits $s \in \Omega \subset \mathcal{S}$ can be approximated by the quantity $\int_{\Omega} n^{(i)}(s)ds$, where $n^{(i)}$ is a continuous function solution of the PDE

$$\partial_t n_t^{(i)}(s) = n_t^{(i)}(s) \left[b^{(i)}(s)(1 - m) - \frac{1}{K} \int_{\mathcal{S}} n_t^{(i)}(\mathbf{s})d\mathbf{s} \right] + m \sum_{j \neq i} b_j(s) \frac{a_{i,j}}{d_j} n_t^{(j)}(s) + \frac{1}{2} \mu \sigma_\mu^2 \Delta_s \left[b^{(i)}(s) n_t^{(i)}(s) \right] \quad (2.4)$$

Equation (2.4) is similar to Eq. (2.3), except that it incorporates an additional term corresponding to mutation processes and that the birth rate is trait dependent. We show how Eq. (2.4) can be reduced to an equivalent two-habitat model under mean field assumption. The mean field approach differs slightly from the setting with no selection because vertices are labelled with Θ_i . Here we assume that vertices with similar habitat types have an equivalent position on the graph (see Fig. S5 for a graphical representation), so that all vertices with habitat type \bullet are characterised by the identical adaptive trait distribution that we denote by \bar{n}^\bullet , and are associated with the birth rate $b^\bullet(s) = b(1 - p(s - \theta_\bullet)^2)$. Let $P(\bullet, \bullet)$ denote the proportion of edges connecting a vertex v_i of type \bullet to a vertex v_j of type \bullet , and let $P(\bullet)$ denote the proportion of vertices v_i of type \bullet . By further assuming that habitats are homogeneously distributed on the graph so that $P(\bullet) = P(\bullet) = \frac{1}{2}$, Eq. (2.4) transforms into

$$\begin{aligned} \partial_t \bar{n}_t^\bullet(s) &= \bar{n}_t^\bullet(s) \left[b^\bullet(s)(1 - m) - \frac{1}{K} \int_{\mathcal{S}} \bar{n}_t^\bullet(\mathbf{s})d\mathbf{s} \right] + \frac{1}{2} \mu \sigma_\mu^2 (\Delta_s b^\bullet \bar{n}_t^\bullet)(s) \\ &\quad + \frac{m}{2} [(1 - r_\Theta) b^\bullet(s) \bar{n}_t^\bullet(s) + (1 + r_\Theta) b^\bullet(s) \bar{n}_t^\bullet(t)] \end{aligned} \quad (2.5)$$

(see Methods), where we define

$$r_\Theta = 2(P(\bullet, \bullet) - P(\bullet, \bullet)) \quad (2.6)$$

as the habitat assortativity of the graph, which ranges from -1 to 1 . When $r_\Theta = -1$, all edges connect dissimilar habitat types (disassortative graph), while as r_Θ tends towards 1 the graph is composed of two clusters of vertices with identical habitat types (assortative graph). Eq. (2.5) can be analysed with the theory of adaptive dynamics [36, 38, 41], a mathematical framework that provides analytical insights by assuming a “trait substitution process”. Following this assumption, the mutation term in Eq. (2.5) is omitted and the phenotypic distribution results in a collection of discrete individual types that are gradually replaced by others until evolutionary stability is reached (see Methods and [36, 38, 41] for details). By applying the theory of adaptive dynamics, we find a critical migration rate m^*

$$m^* = \frac{1}{(1 - r_\Theta)} \frac{4p\theta^2}{(1 + 3p\theta^2)} \quad (2.7)$$

so that when $m > m^*$, a single type of individual exists with adaptive trait $s^* = (\theta_\bullet + \theta_\bullet)/2 = 0$ in the steady state (see Methods for the derivation of Eq. (2.7)). In this case, adaptive differentiation $Q_{ST,s}$ is nil and the average population size is given by $\bar{N} = bK(1 - p\theta)^2$. In contrast, when $m = 0$ and/or $r_\Theta = 1$, all individuals are locally well-adapted with trait Θ_i on v_i , and it follows that the average population size is higher and equal to $\bar{N} = bK$, while adaptive differentiation is maximal and equal to $Q_{ST,s} = \text{Var}(\Theta)/(\text{Var}(\Theta)+0) = 1$. When $0 < m < m^*$, the coexistence of two types of individuals on each vertex v_i is predicted but the calculation of the trait values is more subtle. To understand the effect of m and r_Θ on the local trait distributions and on $Q_{ST,s}$, we therefore leave behind the adaptive dynamics framework and numerically solve Eq. (2.5) by including the mutation term. When $0 < m < m^*$, the local trait distributions are bimodal with peaks corresponding to the two types of individuals predicted by the adaptive dynamics. The highest peak corresponds to the well-adapted individuals, whose adaptation is destabilised by the influx of maladaptive migrants (Fig. 2.3a). This phenomenon is dampened as r_Θ increases, since the proportion of maladaptive migrants is reduced in assortative graphs (Fig. 2.3b). As a consequence, the habitat assortativity r_Θ increases the differentiation $Q_{ST,s}$ when $0 < m < m^*$ (Fig. 2.3c). The simulations further confirm that the adaptive dynamics prediction given by Eq. (2.7) is still valid when the continuous accumulation of mutations is considered, so that for $m > m^*$ the local trait distributions obtained from Eq. (2.5) are unimodal and $Q_{ST,s}$ vanishes (Fig. 2.3a,c). Our analysis of the mean field deterministic approximation Eq. (2.5) therefore demonstrates that assortative graphs present high levels of adaptive differentiation $Q_{ST,s}$. On the other hand, the analysis shows that $Q_{ST,s}$ rapidly declines with increasing m on disassortative graphs, until $Q_{ST,s}$ vanishes when $m > m^*$.

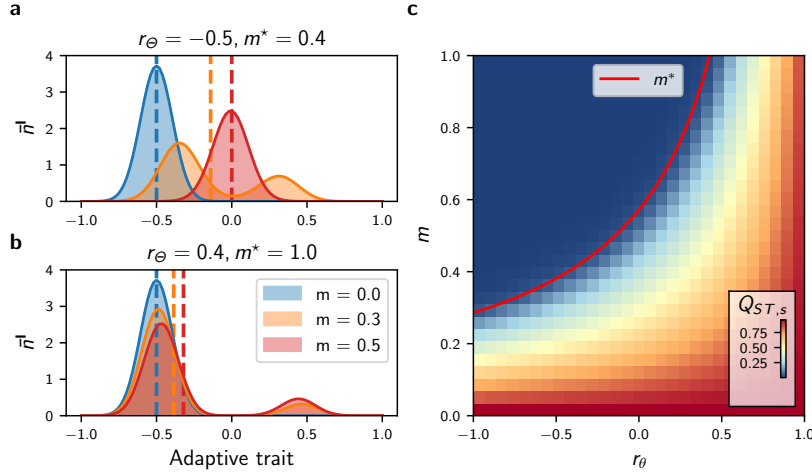


Fig. 2.3: Effect of habitat assortativity r_Θ and migration m on the local adaptive trait distribution \bar{n}^* and on the adaptive differentiation level $Q_{ST,s}$ under the mean field, deterministic approximation Eq. (2.5). (a) Effect of m and r_Θ on \bar{n}^* . Migration induces the apparition of maladaptive individuals (centred around $\theta_+ = 0.5$), which destabilise local adaptation by displacing the mean value of the well-adapted individuals (centred around $\theta_- = -0.5$). Together with the decrease in local adaptation, migration causes a displacement of the mean value of the local trait distribution (represented by the vertical dashed lines), which decreases local population size and adaptive differentiation $Q_{ST,s}$. (b) Similar data for higher r_Θ . Increasing r_Θ increases population size and $Q_{ST,s}$. (c) Effect of r_Θ on $Q_{ST,s}$. The red line indicates the critical migration threshold m^* predicted by Eq. (2.7); $Q_{ST,s}$ vanishes when $m > m^*$.

2.2.5 Effect of graph topology on adaptive differentiation under heterogeneous selection

To generalise the conclusions drawn from the mean field deterministic approximation Eq. (2.5), we generate different Θ -spatial distributions for varying graph topology, and compare outputs of the IBM simulations with those of Eq. (2.5) (see Methods for the details of the simulations). For each combination of Θ -spatial distribution and graph, we compute the habitat assortativity r_Θ , since r_Θ can be generalised from Eq. (2.6) to any graph topology following the original definition of [51] as

$$r_\Theta = \frac{\text{Cov}(\Theta_x, \Theta_\wedge)}{\sigma_{\Theta_x} \sigma_{\Theta_\wedge}} \quad (2.8)$$

where Θ_x and Θ_\wedge denote the sets of habitats found at the toe and tip of each directed vertex of graph V , and $\langle \Theta_x \rangle, \langle \Theta_\wedge \rangle$ and $\sigma_{\Theta_x}, \sigma_{\Theta_\wedge}$ denote their respective means and standard deviations (see Supplementary Note). The mean field deterministic approximation Eq. (2.5) is in very good agreement with the IBM simulations for general graph ensembles at low migration regimes, and captures the response of \bar{N} and $Q_{ST,s}$ to r_Θ (Fig. 2.4). Nonetheless, under high migration regimes, higher levels of $Q_{ST,s}$ are observed in the stochastic simulations compared with the mean field deterministic approximation (Fig. S6). We hypothesize that

this reinforcement is generated by stochastic drift, which must become the main driver of differentiation when local adaptation is lost for $m > m^*$, and perform a multivariate regression analysis to investigate the additional effect of $\langle l \rangle$ and h_d on $Q_{ST,s}$. As expected, the analysis highlights that the effect of $\langle l \rangle$ and h_d are substantial and complement the effect of r_Θ for high m (Fig. 2.5c for graphs with $M = 7$ vertices and Fig. S7a for $M = 9$), further explaining the discrepancies observed (see Table S3).

We extend our analyses to realistic landscapes with a continuum of habitat types by running simulations on graphs obtained from real spatial habitat datasets and by considering mean annual temperature as a proxy for habitat type (see Fig. S8 and Table S4). We also consider simulations accounting for trait-dependent competition to test whether our results hold under more complex ecological processes (see Supplementary Note for the implementation details and Table S5 for the results). The simulations are congruent and show that the effects of r_Θ , h_d and $\langle l \rangle$ are similar under these alternative settings, underlining the robustness of these metrics and the generality of our conclusions. Taken together, these results indicate that under sufficiently strong selection and sufficiently high habitat heterogeneity, adaptive differentiation $Q_{ST,s}$ is mainly driven by habitat assortativity r_Θ . Nonetheless, local adaptation is lost in disassortative graphs when $m > m^*$, such that $\langle l \rangle$ and h_d become complementary determinants of $Q_{ST,s}$ for high migration regimes.

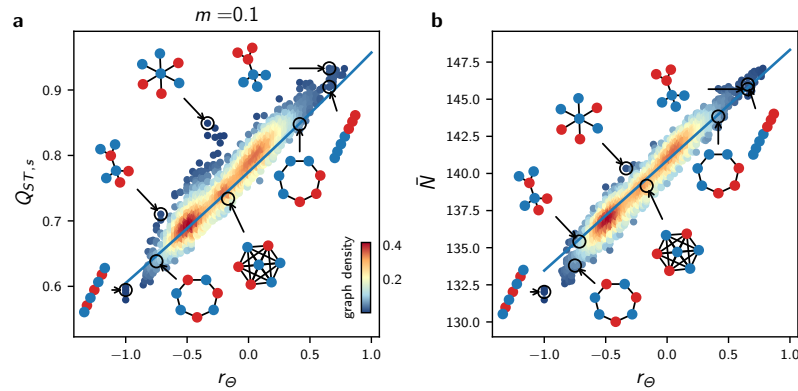


Fig. 2.4: Effect of habitat heterogeneity r_Θ on $Q_{ST,s}$ and average population size \bar{N} for general graph ensembles. (a) Effect of r_Θ on $Q_{ST,s}$ for all undirected connected graphs with $M = 7$ vertices and varying r_Θ , for $m = 0.1$. (b) Effect of r_Θ on average population size \bar{N} for the same simulations. In (a) and (b), each dot represents average results from 5 replicate simulations of the IBM, the colour scale corresponds to the proportion of the graphs with similar x and y axis values (graph density), and the blue lines correspond to results obtained from the mean field approximation Eq. (2.5). Insights from Eq. (2.5) are congruent with the IBM simulations for complex habitat connectivity patterns at low m . Similar results with $m = 0.5$ are presented in Fig. S6.

2.2.6 Effect of habitat assortativity on neutral differentiation under heterogeneous selection

We finally consider a setting with heterogeneous selection where individuals carry both neutral and adaptive traits. With distinct habitat types, selection promotes neutral differentiation by reducing the birth rate of maladaptive migrants, reinforcing the isolation of local populations. We have shown above that adaptive differentiation $Q_{ST,s}$ is driven by habitat assortativity r_Θ , so we expect r_Θ , together with the topological metrics found in the setting with no selection, to influence the level of neutral differentiation $Q_{ST,u}$. We first investigate how the response of $Q_{ST,u}$ to migration compares between the setting with no selection and the setting with heterogeneous selection for graphs with an identical topology. We then examine how the response compares between graphs with an identical topology but different r_Θ . We finally consider simulations on different graphs with varying r_Θ to assess the concurrent effect of $\langle l \rangle$, h_d and r_Θ on $Q_{ST,u}$.

Migration has a fitness cost because maladaptive migrants present lower fitness. Under an equivalent migration regime, migrants therefore have a lower probability of reproduction, increasing the populations' isolation compared with a setting without selection. Simulations with varying m on the complete graph confirm that selection in heterogeneous habitats reinforces $Q_{ST,u}$ compared with a setting without selection (Fig. 2.5a). Nonetheless, previous results show that adaptive differentiation $Q_{ST,s}$ vanishes on a disassortative graph when $m > m^*$, implying that individuals become equally fit in all habitats. In this case, the isolation effect of heterogeneous selection is lost and $Q_{ST,u}$ reaches a similar level as in the setting with no selection for $m > m^*$ (Fig. 2.5a), although $Q_{ST,u}$ is slightly higher in the setting with heterogeneous selection due to a lower population size ($\bar{N} = bK(1 - p\theta)$ vs. $\bar{N} = bK$, see section above and Methods). This suggests that r_Θ reinforces $Q_{ST,u}$, as assortative graphs sustain higher levels of adaptive differentiation (Figs. 2.3 and 2.4). Simulations on the path graph with varying Θ -spatial distribution support this conclusion for high migration regimes, but show the opposite relationship under low migration regimes, where the habitat assortativity r_Θ decreases $Q_{ST,u}$ (Fig. 2.5b). Assortative graphs are composed of large clusters of vertices with similar habitats, within which migrants can circulate without fitness losses. Local neutral trait distributions become more correlated within these clusters, resulting in a decline in $Q_{ST,u}$ for assortative graphs compared with disassortative graphs. Figure 2.5b therefore highlights the ambivalent effect of r_Θ on $Q_{ST,u}$. r_Θ reinforces $Q_{ST,u}$ by favouring adaptive differentiation, but also decreases $Q_{ST,u}$ by decreasing population isolation within clusters of vertices with the same habitat type.

We compare the effect of r_Θ on $Q_{ST,u}$ to the effect of the topology metrics $\langle l \rangle$ and h_d found in the setting with no selection using a multivariate regression analysis on simulation results obtained for different graphs with varying Θ -spatial distribution (Fig. 2.5d for graphs with $M = 7$ vertices and Fig. S7b for $M = 9$). The multivariate model explains the discrepancies in $Q_{ST,u}$ across the simulations for low and high migration regimes (see Table S3 for details), and we find that r_Θ , $\langle l \rangle$ and h_d contribute similarly to neutral differentiation. Hence, the effects of r_Θ and the topology metrics $\langle l \rangle$ and h_d add up under heterogeneous selection. A change in sign of the standardized effect of r_Θ on $Q_{ST,s}$ for low and high migration regimes verifies that the ambivalent effect of r_Θ on $Q_{ST,u}$ found on the path

graph holds for general graph ensembles. Simulations with trait-dependent competition and simulations on realistic graphs with a continuum of habitat types equally confirm the ambivalent effect of r_Θ and further support the complementary effect of $\langle l \rangle$ and h_d on $Q_{ST,u}$ (see Fig. S8). $\langle l \rangle$ and h_d therefore drive neutral differentiation with and without heterogeneous selection. r_Θ becomes an additional determinant of neutral differentiation under heterogeneous selection. In contrast to the non-ambivalent, positive effect of habitat assortativity on adaptive differentiation, r_Θ can amplify or depress neutral differentiation depending on the migration regime considered.

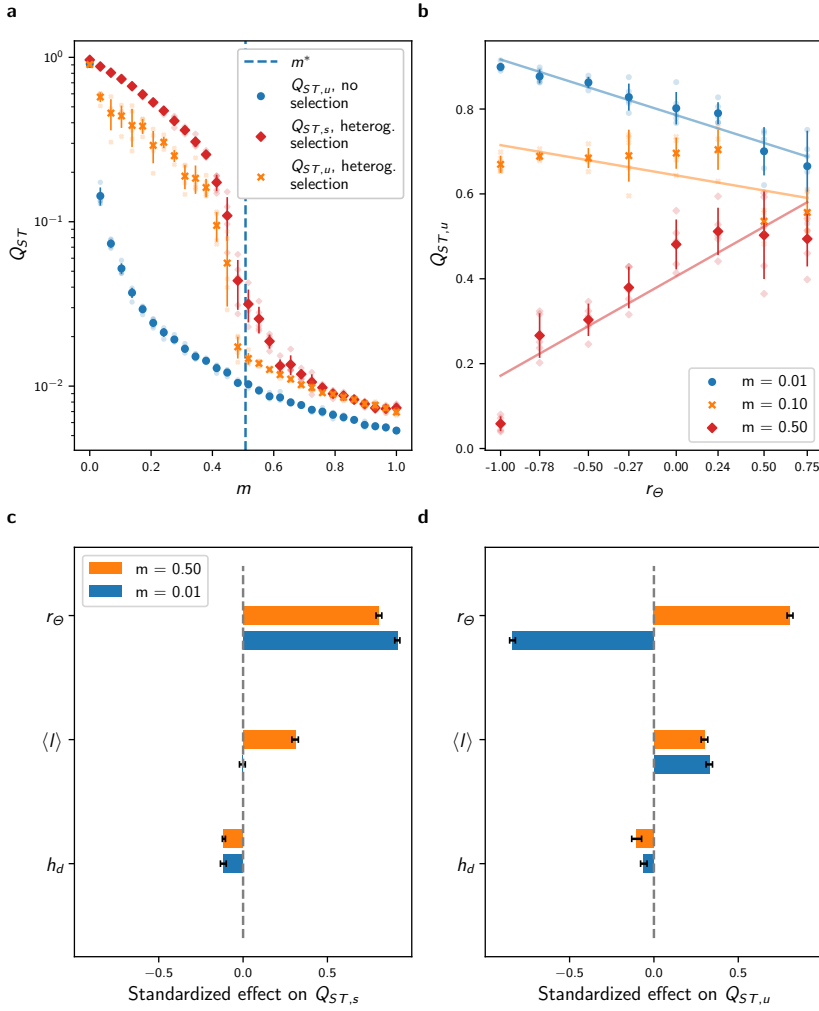


Fig. 2.5: Effect of r_Θ , $\langle I \rangle$ and h_d on $Q_{ST,s}$ and $Q_{ST,u}$ in the setting with heterogeneous selection. (a) Comparison of the response of $Q_{ST,u}$ to migration with the response of $Q_{ST,u}$ in the setting with no selection for the complete graph. The dashed vertical blue line corresponds to the critical migration regime m^* predicted by Eq. (2.7). Heterogeneous selection increases $Q_{ST,u}$ when $m < m^*$, but local adaptation is lost when $m > m^*$, and in this case $Q_{ST,u}$ reaches similar levels as $Q_{ST,u}$ in the setting with no selection. (b) Response of $Q_{ST,u}$ to r_Θ and migration for the path graph. r_Θ correlates positively with $Q_{ST,u}$ for high m , but correlates negatively for low m . In (a–b), each plain dot represents average results from 5 replicate simulations, the bars represent one standard deviation, and each fade dot represents a single replicate value. (c–d) Standardized effect of h_d , $\langle I \rangle$ and r_Θ on $Q_{ST,s}$ and $Q_{ST,u}$ obtained from a multivariate regression model independently fitted for low and high migration regimes on average results from 5 replicate simulations of the IBM on all undirected connected graphs with $M = 7$ vertices and varying r_Θ (see Methods). The ambivalence of the effect of r_Θ on $Q_{ST,u}$ found for the path graph holds for general graph ensembles and adds up to that of $\langle I \rangle$ and h_d . Error bars show 95% confidence intervals. Analogous results on graphs with $M = 9$ vertices are presented in Fig. S7 and all regression details can be found in Table S3.

2.3 Discussion

Using analytical tools and simulations, we have built upon a graph representation of landscapes and a stochastic individual-based model to investigate how landscape features drive phenotypic differentiation. Our study is based on a first principles modelling approach [29] describing the stochastic dynamics of individuals and capturing the interplay between population dynamics, phenotypic evolution and spatial dynamics in heterogeneous habitats. In contrast to metacommunity models [17, 18, 19, 20, 21, 22, 23] and evolutionary metacommunity models [26, 27], we have focused on differentiation at the population level. Quantitative genetics and population genetics studies have investigated the effect of topology on differentiation under the assumption of non-overlapping generations, constant population sizes and regular spatial structures [31, 48, 33, 34, 52]. Generalising beyond these assumptions, our modelling framework accounts for population dynamics and includes competition and frequency-dependent selection. The systematic investigation of the effect of topology on differentiation over general graph ensembles and under different ecological settings shows that average path length $\langle l \rangle$, homogeneity in vertex degree h_d and habitat assortativity r_Θ contribute equally to differentiation. These results support correlative studies that have associated population differentiation [44, 53] and species richness [54, 4, 55, 56, 57, 58, 5, 59] with a variety of metrics used as surrogates for connectivity, connectivity heterogeneity and habitat heterogeneity. To further our understanding of the origin of spatial biodiversity patterns, the contribution of landscape properties to discrepancies in population differentiation could be investigated at large scales by (i) using techniques to project real landscapes on graphs (see Fig. S8a–b); (ii) characterising the landscape features with $\langle l \rangle$, h_d and r_Θ ; and (iii) relating the obtained metrics maps to observation data. More generally, the proposed eco-evolutionary model on spatial graphs could be combined with approximate bayesian computation to estimate ecological, spatial and evolutionary processes of real populations from observation data, similarly to [60]. This approach might improve current inferential techniques based on models that do not account for competition nor heterogeneous selection (see e.g. [61]). Overall, our results point to topology metrics that can connect spatial biodiversity patterns to the generating eco-evolutionary and spatial processes.

In the absence of selection, neutral differentiation is more pronounced on graphs with a high average path length $\langle l \rangle$, but is also negatively associated with homogeneity in degree h_d (Fig. 2.2c–d). $\langle l \rangle$ generalises the concept of dimensionality in [48, 33, 34], where it is shown that differentiation is lower for two-dimensional grid graphs compared with path graphs. $\langle l \rangle$ also closely relates to the concept of resistance distance shown theoretically and empirically to drive genetic differentiation [62, 53]. At the species level, a similar effect of $\langle l \rangle$ on β -diversity (pairwise differences in species composition) has been reported with the graph metacommunity model of [21] and with the graph eco-evolutionary metacommunity model of [26]. Accounting for population dynamics and specifically including competition processes, we have shown that not only $\langle l \rangle$ but also h_d affects neutral phenotypic differentiation (Fig. 2.2c,d). Our model realistically assumes that population growth is limited by the local

carrying capacity. The latter becomes saturated on highly connected vertices in irregular graphs, an effect that has been experimentally documented in microcosm experiments [63]. As a consequence, central vertices behave as bottlenecks and amplify the isolation of peripheral vertices [13]. The role of h_d cannot be captured with classical metapopulation and quantitative genetics models or with models of evolutionary dynamics in graphs, as they assume constant population size. This behaviour should be prevalent in patchy landscapes where interspecific competition is high because of limiting resources. Our study highlights that heterogeneity in connectivity can reinforce differentiation patterns through the creation of unbalanced migration fluxes which affect ecological equilibrium.

Habitat assortativity r_Θ is a useful indicator for assessing how the spatial distribution of habitat types modulates local adaptation and adaptive differentiation in complex landscapes [64]. While adaptation has been extensively studied along environmental gradients [65, 32, 66, 67, 40, 68, 35], landscapes can be patchy and it is unrealistic to assume regularity [16]. Our model of heterogeneous selection on spatial graphs extends the two-habitat setting investigated in [36, 52, 38, 41] and captures irregularity in connectivity between distinct habitats [16]. Similarly to the aforementioned studies, we have found a critical migration regime m^* that dictates the possibility of adaptation. Equation (2.7) indicates that m^* increases with increasing selection strength p and with increasing environmental heterogeneity θ , the latter playing a similar role as the slope of the environmental gradient in [65, 32, 67, 40]. Local adaptation would consequently be sustained under higher migration regimes following an increase in these parameters. Additionally, the critical migration regime m^* in Eq. (2.7) involves the habitat assortativity r_Θ , which must be regarded as a measure of habitat spatial auto-correlation based on the dispersal range of a species [64]. Our results indicate that for general habitat distributions, r_Θ is the main determinant of adaptive differentiation under sufficiently strong selection p and high habitat heterogeneity θ , irrespective of the graph topology (Fig. 2.5c, Fig. S7a and Fig. S8). As p decreases, however, the effect of stochastic drift on $Q_{ST,s}$ should increase, and in this case the topology metrics $\langle l \rangle$ and h_d should become the most important determinants of $Q_{ST,s}$. Our results predict that in landscapes with heterogeneous habitats and where selection is strong, populations structured over assortative habitats are larger, support higher adaptive differentiation, and can be locally well-adapted even in the case where migration rates are high.

Spatial eco-evolutionary feedbacks in heterogeneous habitats can critically affect differentiation [64]. While most eco-evolutionary studies have investigated diversification by considering a unique adaptive trait [35, 66, 67, 40], distinguishing between neutral and adaptive processes is crucial [9] and our work underlines the distinct responses of neutral and adaptive differentiation to landscape features (Fig. 2.5c vs. Fig. 2.5d). Our study builds upon recent mathematical models that consider the co-evolution of neutral and adaptive traits [42, 43] and extends those works to a spatial context. Our work provides an analytical framework to the concept of isolation by environment (IBE) [13], which has been suggested to be one of the most important mechanisms governing differentiation in nature [14]. Heterogeneous selection leads to more isolation by modifying the fitness of migrants [40], which further reduces gene flow [64] and therefore affects the level of neutral differentiation (Fig. 2.5a) [15]. Our work proposes a mechanism by which habitat assortativity, relative to the migration regime, controls the direction of the effect of

habitat heterogeneity on differentiation (Fig. 2.5d). Patchy, heterogeneous habitats can promote neutral differentiation as a result of selection that reduces effective migration [59]. Nonetheless, adaptive differentiation decreases substantially when migration is high relative to the critical migration regime m^* . In this case, neutral differentiation should be higher in landscapes with more aggregated habitats [64]. Our study suggests that habitat assortativity must be considered for a complete understanding of differentiation in complex environments [59].

In conclusion, we have established how differentiation can emerge at the population level from eco-evolutionary feedbacks in complex landscapes by using an analytical description of micro-evolutionary processes explicitly accounting for spatial dynamics over graphs. Our study formalises how differentiation emerges from the interplay between spatial dynamics, the co-evolution of neutral and adaptive traits, and landscape properties. Connectivity and habitat assortativity emerge as core determinants of differentiation in spatial graphs. These results resonate with empirical findings and previous theoretical works. Our study further stresses that habitat assortativity can depress or foster neutral differentiation depending on the migration regime. Additionally, our work highlights that heterogeneity in connectivity is an equally strong determinant of differentiation because highly connected habitats behave as bottlenecks, increasing the isolation of peripheral habitats. The present approach offers a promising framework for studying complex adaptive systems, as it can elucidate how macroscopic properties emerge from microscopic processes acting upon agents structured over complex spatio-evolutionary structures.

2.4 Methods

2.4.1 Mean field approximation

In the setting with no selection, the mean field approach involves the assumption that all vertices having the same degree are equivalent. For this, let $P(k, k')$ denote the proportion of edges that map a vertex with degree k to a vertex with degree k' , and consider the average population size $\bar{N}_t^{(k)}$ in each vertex with degree k at time t . An individual has probability $P(k, k')/k'$ to migrate from a vertex with degree k' to a vertex with degree k . Viewing $a_{i,j}/d_j$ as the probability that an individual on v_i chosen for migration moves to v_j , Eq. (2.3) then transforms into

$$\partial_t \bar{N}_t^{(k)} = \bar{N}_t^{(k)} \left[b(1-m) - \frac{\bar{N}_t^{(k)}}{K} \right] + mbk \sum_{k' \in V} \frac{P(k, k')}{k'} \bar{N}_t^{(k')} \quad (2.9)$$

Assuming uncorrelated graphs for which $P(k, k')/k' = P(k')k'/\langle k \rangle$, where $\langle k \rangle$ denotes the average degree of the graph [49], yields

$$\partial_t \bar{N}_t^{(k)} = \bar{N}_t^{(k)} \left[b(1-m) - \frac{\bar{N}_t^{(k)}}{K} \right] + mb \frac{k}{\langle k \rangle} \bar{N}_t \quad (2.10)$$

where

$$\bar{N}_t = \sum_k P(k) \bar{N}_t^{(k)}. \quad (2.11)$$

When solving for the stationary state and setting $m = 1$, one obtains $\bar{N}^{(k)} = \sqrt{bK \frac{k}{\langle k \rangle} \bar{N}}$ from Eq. (2.10). Combining this with Eq. (2.11) yields

$$\bar{N} = bK \langle \sqrt{k} \rangle^2 / \langle k \rangle \quad (2.12)$$

In the setting with heterogeneous selection, the mean field approach involves the assumption that all vertices with a similar habitat are equivalent. In this case, an individual from a vertex of habitat type \bullet has the probability $P(\bullet, \bullet)/P(\bullet)$ of migrating to a vertex of type \bullet , and therefore Eq. (2.4) transforms into

$$\begin{aligned} \partial_t \bar{n}_t^\bullet(s) &= \bar{n}_t^\bullet(s) \left[b^\bullet(s)(1-m) - \frac{1}{K} \int_S \bar{n}_t^\bullet(s) d\mathbf{s} \right] + \frac{1}{2} \mu \sigma_\mu^2 \Delta_s [b^\bullet(s) \bar{n}_t^\bullet(s)] \\ &\quad + m \sum_{i \in \{\bullet, \bullet\}} b_i(s) \frac{P(\bullet, i)}{P(i)} \bar{n}_t^i(s) \end{aligned} \quad (2.13)$$

Considering that $P(\bullet) = P(\bullet) = \frac{1}{2}$ (habitats are equally distributed), $P(\bullet, \bullet) + P(\bullet, \bullet) = P(\bullet)$ (sum of conditional expectations), and $r_\Theta = 2(P(\bullet, \bullet) - P(\bullet, \bullet))$ (Eq. (2.6)), one obtains

$$P(\bullet, \bullet) = \frac{1}{4}(1 - r_\Theta) \quad \text{and} \quad P(\bullet, \bullet) = \frac{1}{4}(1 + r_\Theta) \quad (2.14)$$

Combining Eq. (2.14) with Eq. (2.13) yields Eq. (2.5). We show in the Supplementary Note how one can derive Eq. (2.6) from the general definition of assortativity given in Eq. (2.8) and initially introduced in [51].

2.4.2 Adaptive dynamics on graphs

The adaptive dynamics theory considers a monomorphic population that evolves following a “trait substitution process” [36]. Accordingly, the trait s of the monomorphic metapopulation evolves gradually along the direction given by its fitness gradient, until it reaches a singular strategy s^* for which the fitness gradient vanishes. By omitting the mutation term, Eq. (2.6) can be written in the matrix form

$$\partial_t \bar{\mathbf{n}}_t(s) = M(s, \bar{\mathbf{N}}_t) \bar{\mathbf{n}}_t(s) \quad (2.15)$$

where $\bar{\mathbf{n}}_t = (\bar{n}_t^\bullet, \bar{n}_t^\bullet)$ and $\bar{\mathbf{N}}_t = (\bar{N}_t^\bullet, \bar{N}_t^\bullet)$ are the vectors containing the population densities and the population size on each habitat type, and

$$M(s, \bar{\mathbf{N}}) = \begin{bmatrix} \mathbf{r}^\bullet(s, \bar{N}^\bullet) & \frac{m}{2}(1 - r_\Theta)b^\bullet(s) \\ \frac{m}{2}(1 - r_\Theta)b^\bullet(s) & \mathbf{r}^\bullet(s, \bar{N}^\bullet) \end{bmatrix} \quad (2.16)$$

is the so-called projection matrix [36], with $\mathbf{r}^\bullet(s, \bar{N}^\bullet) = b^\bullet(s)(1 + \frac{m}{2}(r_\Theta - 1)) - \bar{N}^\bullet/K$. The overall fitness of individuals with trait s is the leading eigenvalue of M , which we denote with $\lambda(s, \bar{\mathbf{N}})$. We obtain the singular strategy s^* by setting the fitness gradient $\frac{\partial \lambda}{\partial s}(s, \bar{\mathbf{N}}) = 0$,

from which we further obtain the demographic equilibrium \bar{N}^{s^*} . Because of symmetries, we must have $\bar{N}^{\bullet,s^*} = \bar{N}^{\bullet,s^*}$ and $s^* = \frac{\theta_\bullet + \theta_\bullet}{2} = 0$, such that $\bar{N}^{\bullet,s^*} = \bar{N}^{\bullet,s^*} = bK(1 - p\theta^2)$. s^* is said to be evolutionary stable if no mutants can invade, i.e. if s^* locally maximises the fitness of a mutant with trait y in the resident population with trait s^* , given by $\lambda(y, \bar{N}^{s^*})$ (see [36] for details). One can show that $\left[\frac{\partial \lambda}{\partial y}(y, \bar{N}^{s^*}) \right]_{y=s^*} = 0$ and the condition for evolutionary stability becomes $\left[\frac{\partial^2 \lambda}{\partial y^2}(y, \bar{N}^{s^*}) \right]_{y=s^*} < 0$. We compute and simplify this inequality through computer algebra (see Mathematica notebook provided in the simulation code), which leads to Eq. (2.7).

2.4.3 Numerical simulations

The model was implemented in a multi-purpose Julia package called `EvoId.jl`, available at <https://github.com/vboussange/EvoId.jl>. For each result presented, $b = 1$, local carrying capacity $K = 150$, selection strength $p = 1$, mutation rate $\mu = 0.1$, mutation range $\sigma_\mu = 5 \cdot 10^{-2}$, and total time span $t = 1000$. This parameter choice made it possible to discard transient dynamics while obtaining results in a reasonable computational time (see Fig. S9). In settings (1) and (2), we ran simulations on all of the 853 undirected connected graphs with $M = 7$ vertices and on 1126 of the 261,080 undirected connected graphs with $M = 9$ vertices, listed at <http://oeis.org/A001349>. Graphs with $M = 9$ vertices were selected with a stratified sampling method: we randomly sampled without replacement a maximum of 50 graphs for each class of graphs with an equal number of vertices. For the setting with heterogeneous selection, we generated the labeled graphs by randomly generating Θ -spatial distributions, and by using a stratified sampling strategy to select without replacement at most 3 and 2 Θ -spatial distributions corresponding to the quartiles of the r_θ values obtained, respectively for graphs with $M = 7$ and $M = 9$ vertices. This sampling strategy allowed to obtain a uniform distribution of the topology metrics investigated in the study, and therefore permitted to correctly represent the population of graphs to investigate their effect on differentiation. We then computed $Q_{ST,u}$ and $Q_{ST,s}$, which we further averaged over the last time steps and across the replicates. Since the dynamics of $Q_{ST,u}$ is characterised by large quadratic variations, we simulated individuals with $d = 300$ neutral traits, where each trait can independently be affected by mutations. $Q_{ST,u}$ values presented were then obtained from the average $Q_{ST,u}$ for each trait. This reduced the variance of the numerical simulations and is also biologically meaningful because populations are characterised by many traits, most of which are neutral [9]. As initial conditions, MK individuals were homogeneously distributed over all of the vertices, with traits centred on 0 and with standard deviation σ_μ . Graph metrics used for the meta-analysis were calculated using the `LightGraphs.jl` library [69]. We numerically solved the PDEs with a finite difference scheme using `DifferentialEquations.jl` [70], ensuring that the domain was large enough to avoid border effects.

2.4.4 Statistics and reproducibility

Statistical analyses were conducted in Julia using **StatsKit.jl**. All simulations can be exactly reproduced from the code available at <https://github.com/vboussange/differentiation-in-spatial-graphs>.

Data availability

The data underlying our figures is available at <https://github.com/vboussange/differentiation-in-spatial-graphs>.

Code availability

The simulation code is available at <https://github.com/vboussange/differentiation-in-spatial-graphs>.

Author contributions

V.B. and L.P. designed research; V.B. performed research; V.B. and L.P. wrote the paper.

Acknowledgements

We thank Thomas Poulet, Sylvian Billiard, Sepideh Mirrahimi, Heike Lischke, Joshua Payne, Conor Waldock, Yaquan Chang, Flora Desmet, Benjamin Flück and Alexander Skeels for helpful discussions and comments on the manuscript. L.P. was supported by the Swiss National Science Foundation grant (N° 310030_188550). We thank two anonymous reviewers for constructive comments and valuable suggestions on a previous version of this article.

References

- [1] S. P. Hubbell. *The unified neutral theory of biodiversity and biogeography*. Monographs in Population Biology 32. Princeton [etc]: Princeton University Press, 2001.
- [2] C. Rahbek et al. “Building mountain biodiversity: Geological and evolutionary processes”. In: *Science* 365.6458 (2019), pp. 1114–1119. DOI: 10.1126/science.aax0151.
- [3] W.-N. Ding et al. “Ancient orogenic and monsoon-driven assembly of the world’s richest temperate alpine flora”. In: *Science* 369.6503 (2020), pp. 578–581. DOI: 10.1126/science.abb4484.

- [4] M. S. Dias et al. “Global imprint of historical connectivity on freshwater fish biodiversity”. In: *Ecology Letters* 17.9 (2014). Ed. by M. Anderson, pp. 1130–1140. DOI: 10.1111/ele.12319.
- [5] J.-F. Guégan, S. Lek, and T. Oberdorff. “Energy availability and habitat heterogeneity predict global riverine fish diversity”. In: *Nature* 391.6665 (1998), pp. 382–384. DOI: 10.1038/34899.
- [6] S. A. Levin. “Complex adaptive systems: Exploring the known, the unknown and the unknowable”. In: *Bulletin of the American Mathematical Society* 40.01 (2002), pp. 3–20. DOI: 10.1090/S0273-0979-02-00965-5.
- [7] J. S. Cabral, L. Valente, and F. Hartig. “Mechanistic simulation models in macroecology and biogeography: state-of-art and prospects”. In: *Ecography* 40.2 (2017), pp. 267–280. DOI: 10.1111/ecog.02480.
- [8] S. Lion. “Moment equations in spatial evolutionary ecology”. In: *Journal of Theoretical Biology* 405 (2016), pp. 46–57. DOI: 10.1016/j.jtbi.2015.10.014.
- [9] R. Holderegger, U. Kamm, and F. Gugerli. “Adaptive vs. neutral genetic diversity: implications for landscape genetics”. In: *Landscape Ecology* 21.6 (2006), pp. 797–807. DOI: 10.1007/s10980-005-5245-9.
- [10] M. Slatkin. “Isolation by distance in equilibrium and non-equilibrium populations”. In: *Evolution* 47.1 (1993), pp. 264–279. DOI: 10.1111/j.1558-5646.1993.tb01215.x.
- [11] U. Dieckmann and M. Doebeli. “On the origin of species by sympatric speciation”. In: *Nature* 400.6742 (1999), pp. 354–357. DOI: 10.1038/22521.
- [12] N. L. Kaplan, R. Hudson, and C. H. Langley. “The “hitchhiking effect” revisited.” In: *Genetics* 123.4 (1989), pp. 887–899. DOI: 10.1093/genetics/123.4.887.
- [13] L. Orsini et al. “Drivers of population genetic differentiation in the wild: Isolation by dispersal limitation, isolation by adaptation and isolation by colonization”. In: *Molecular Ecology* 22.24 (2013), pp. 5983–5999. DOI: 10.1111/mec.12561.
- [14] I. J. Wang and G. S. Bradburd. “Isolation by environment”. In: *Molecular Ecology* 23.23 (2014), pp. 5649–5662. DOI: 10.1111/mec.12938.
- [15] D. Garant, S. E. Forde, and A. P. Hendry. “The multifarious effects of dispersal and gene flow on contemporary adaptation”. In: *Functional Ecology* 21.3 (2007), pp. 434–443. DOI: 10.1111/j.1365-2435.2006.01228.x.

- [16] M. R. Dale and M. Fortin. “From graphs to spatial graphs”. In: *Annual Review of Ecology, Evolution, and Systematics* 41 (2010), pp. 21–38. DOI: 10.1146/annurev-ecolsys-102209-144718.
- [17] M. D. Holland and A. Hastings. “Strong effect of dispersal network structure on ecological dynamics”. In: *Nature* 456.7223 (2008), pp. 792–794. DOI: 10.1038/nature07395.
- [18] L. J. Gilarranz and J. Bascompte. “Spatial network structure and metapopulation persistence”. In: *Journal of Theoretical Biology* 297 (2012), pp. 11–16. DOI: 10.1016/j.jtbi.2011.11.027.
- [19] L. Mari et al. “Metapopulation persistence and species spread in river networks”. In: *Ecology Letters* 17.4 (2014). Ed. by F. Jordán, pp. 426–434. DOI: 10.1111/ele.12242.
- [20] D. Gravel, F. Massol, and M. A. Leibold. “Stability and complexity in model meta-ecosystems”. In: *Nature Communications* 7.1 (2016), p. 12457. DOI: 10.1038/ncomms12457.
- [21] F. Carrara et al. “Dendritic connectivity controls biodiversity patterns in experimental metacommunities”. In: *Proceedings of the National Academy of Sciences of the United States of America* 109.15 (2012), pp. 5761–5766. DOI: 10.1073/pnas.1119651109.
- [22] P. L. Thompson, B. Rayfield, and A. Gonzalez. “Loss of habitat and connectivity erodes species diversity, ecosystem functioning, and stability in metacommunity networks”. In: *Ecography* 40.1 (2017), pp. 98–108. DOI: 10.1111/ecog.02558.
- [23] Y. Suzuki and E. P. Economo. “From species sorting to mass effects: spatial network structure mediates the shift between metacommunity archetypes”. In: *Ecography* (2021), p. 05453. DOI: 10.1111/ecog.05453.
- [24] F. Pelletier, D. Garant, and A. Hendry. “Eco-evolutionary dynamics”. eng. In: *Philosophical Transactions of the Royal Society of London. Series B, Biological Sciences* 364.1523 (2009), pp. 1483–1489. DOI: 10.1098/rstb.2009.0027.
- [25] J. Tkadlec et al. “Population structure determines the tradeoff between fixation probability and fixation time”. In: *Communications Biology* 2.1 (2019), p. 138. DOI: 10.1038/s42003-019-0373-y.
- [26] E. P. Economo and T. H. Keitt. “Species diversity in neutral metacommunities: a network approach”. In: *Ecology Letters* 11.1 (2007), 071117033013001–???. DOI: 10.1111/j.1461-0248.2007.01126.x.

- [27] E. P. Economo and T. H. Keitt. “Network isolation and local diversity in neutral metacommunities”. In: *Oikos* 119.8 (2010), pp. 1355–1363. DOI: 10.1111/j.1600-0706.2010.18272.x.
- [28] R. Muneepetarakul et al. “Neutral metacommunity models predict fish diversity patterns in Mississippi–Missouri basin”. In: *Nature* 453.7192 (2008), pp. 220–222. DOI: 10.1038/nature06813.
- [29] N. Champagnat, R. Ferrière, and S. Méléard. “Unifying evolutionary dynamics: From individual stochastic processes to macroscopic models”. In: *Theoretical Population Biology* 69.3 (2006), pp. 297–321. DOI: 10.1016/j.tpb.2005.10.004.
- [30] V. Bansaye and S. Méléard. “Some stochastic models for structured populations : scaling limits and long time behavior”. In: *Stochastic Models for Structured Populations: Scaling Limits and Long Time Behavior* (2015), pp. 1–107. DOI: 10.1007/978-3-319-21711-6. arXiv: 1506.04165.
- [31] R. Bürger. *The mathematical theory of selection, recombination, and mutation*. eng. Wiley series in mathematical and computational biology. Chichester [etc]: J. Wiley, 2000.
- [32] M. Slatkin. “Spatial patterns in the distributions of polygenic characters”. In: *Journal of Theoretical Biology* 70.2 (1978), pp. 213–228. DOI: 10.1016/0022-5193(78)90348-X.
- [33] R. Lande. “Isolation by distance in a quantitative trait”. In: *Genetics* 128.2 (1991), pp. 443–452.
- [34] T. Nagylaki. “Geographical variation in a quantitative character.” In: *Genetics* 136.1 (1994), pp. 361–81.
- [35] M. Doebeli and U. Dieckmann. “Speciation along environmental gradients”. In: *Nature* 421.6920 (2003), pp. 259–264. DOI: 10.1038/nature01274.
- [36] G. Meszéna, I. Czibula, and S. Geritz. “Adaptive Dynamics in a 2-Patch Environment: A Toy Model for Allopatric and Parapatric Speciation”. In: *Journal of Biological Systems* 05.02 (1997), pp. 265–284. DOI: 10.1142/S0218339097000175.
- [37] R. Aguilée, D. Claessen, and A. Lambert. “Adaptive radiation driven by the interplay of eco-evolutionary and landscape dynamics”. In: *Evolution* 67.5 (2012), no–no. DOI: 10.1111/evo.12008.
- [38] F. Débarre, O. Ronce, and S. Gandon. “Quantifying the effects of migration and mutation on adaptation and demography in spatially heterogeneous environments”. In: *Journal of Evolutionary Biology* 26.6 (2013), pp. 1185–1202. DOI: 10.1111/jeb.12132.

- [39] J. Wickman et al. “Determining selection across heterogeneous landscapes: A perturbation-based method and its application to modeling evolution in space”. In: *The American Naturalist* 189.4 (2017), pp. 381–395. DOI: 10.1086/690908.
- [40] J. Polechová. “Is the sky the limit? On the expansion threshold of a species’ range”. In: *PLoS Biology* 16.6 (2018), pp. 1–18. DOI: 10.1371/journal.pbio.2005372.
- [41] S. Mirrahimi and S. Gandon. “Evolution of specialization in heterogeneous environments: equilibrium between selection, mutation and migration”. In: *Genetics* 214.2 (2020), pp. 479–491. DOI: 10.1534/genetics.119.302868.
- [42] S. Billiard et al. “Stochastic dynamics of adaptive trait and neutral marker driven by eco-evolutionary feedbacks”. In: *Journal of Mathematical Biology* 71.5 (2015), pp. 1211–1242. DOI: 10.1007/s00285-014-0847-y. arXiv: 1310.6274.
- [43] N. Anceschi et al. “Neutral and niche forces as drivers of species selection”. In: *Journal of Theoretical Biology* 483 (2019), p. 109969. DOI: 10.1016/j.jtbi.2019.07.021.
- [44] S. Manel et al. “Landscape genetics: combining landscape ecology and population genetics”. In: *Trends in Ecology & Evolution* 18.4 (2003), pp. 189–197. DOI: 10.1016/S0169-5347(03)00008-9.
- [45] R. Lande. “NEUTRAL THEORY OF QUANTITATIVE GENETIC VARIANCE IN AN ISLAND MODEL WITH LOCAL EXTINCTION AND COLONIZATION”. In: *Evolution* 46.2 (1992), pp. 381–389. DOI: 10.1111/j.1558-5646.1992.tb02046.x.
- [46] M. C. Whitlock. “Evolutionary inference from Q ST”. In: *Molecular Ecology* 17.8 (2008), pp. 1885–1896. DOI: 10.1111/j.1365-294X.2008.03712.x.
- [47] D. T. Gillespie. “A general method for numerically simulating the stochastic time evolution of coupled chemical reactions”. In: *Journal of Computational Physics* 22.4 (1976), pp. 403–434. DOI: 10.1016/0021-9991(76)90041-3.
- [48] M Kimura and G. H. Weiss. “The stepping stone model of population structure and the decrease of genetic correlation with distance.” In: *Genetics* 49.4 (1964), pp. 561–76. DOI: 10.1093/oxfordjournals.molbev.a025590.
- [49] V. Colizza, R. Pastor-Satorras, and A. Vespignani. “Reaction–diffusion processes and metapopulation models in heterogeneous networks”. In: *Nature Physics* 3.4 (2007), pp. 276–282. DOI: 10.1038/nphys560. arXiv: 0703129 [cond-mat].

- [50] G. Bounova and O. de Weck. “Overview of metrics and their correlation patterns for multiple-metric topology analysis on heterogeneous graph ensembles”. In: *Physical Review E* 85.1 (2012), p. 016117. DOI: 10.1103/PhysRevE.85.016117.
- [51] M. E. J. Newman. “Mixing patterns in networks”. In: *Physical Review E* 67.2 (2003), p. 026126. DOI: 10.1103/PhysRevE.67.026126. arXiv: 0209450 [cond-mat].
- [52] S. Yeaman and S. P. Otto. “Establishment and maintenance of adaptive genetic divergence under migration, selection, and drift”. In: *Evolution* 65.7 (2011), pp. 2123–2129. DOI: 10.1111/j.1558-5646.2011.01277.x.
- [53] B. H. McRae and P. Beier. “Circuit theory predicts gene flow in plant and animal populations”. In: *Proceedings of the National Academy of Sciences* 104.50 (2007), pp. 19885–19890. DOI: 10.1073/pnas.0706568104.
- [54] C. Liu et al. “Mountain metacommunities: climate and spatial connectivity shape ant diversity in a complex landscape”. In: *Ecography* 41.1 (2018), pp. 101–112. DOI: 10.1111/ecog.03067.
- [55] C. Rahbek and G. R. Graves. “Multiscale assessment of patterns of avian species richness”. In: *Proceedings of the National Academy of Sciences of the United States of America* 98.8 (2001), pp. 4534–4539. DOI: 10.1073/pnas.071034898.
- [56] H. Kreft and W. Jetz. “Global patterns and determinants of vascular plant diversity”. In: *Proceedings of the National Academy of Sciences of the United States of America* 104.14 (2007), pp. 5925–5930. DOI: 10.1073/pnas.0608361104.
- [57] R. G. Davies et al. “Topography, energy and the global distribution of bird species richness”. In: *Proceedings of the Royal Society B: Biological Sciences* 274.1614 (2007), pp. 1189–1197. DOI: 10.1098/rspb.2006.0061.
- [58] J. A. Veech and T. O. Crist. “Habitat and climate heterogeneity maintain beta-diversity of birds among landscapes within ecoregions”. In: *Global Ecology and Biogeography* 16.5 (2007), pp. 650–656. DOI: 10.1111/j.1466-8238.2007.00315.x.
- [59] A. Stein, K. Gerstner, and H. Kreft. “Environmental heterogeneity as a universal driver of species richness across taxa, biomes and spatial scales”. In: *Ecology Letters* 17.7 (2014), pp. 866–880. DOI: 10.1111/ele.12277.
- [60] C. Lepers et al. “Inference with selection, varying population size, and evolving population structure: application of ABC to a forward–backward coalescent process with interactions”. In: *Heredity* 126.2 (2021), pp. 335–350. DOI: 10.1038/s41437-020-00381-x. arXiv: 1910.10201.

- [61] D. Petkova, J. Novembre, and M. Stephens. “Visualizing spatial population structure with estimated effective migration surfaces”. In: *Nature Genetics* 48.1 (2015), pp. 94–100. DOI: 10.1038/ng.3464.
- [62] B. H. McRae. “ISOLATION BY RESISTANCE”. In: *Evolution* 60.8 (2006), p. 1551. DOI: 10.1554/05-321.1.
- [63] F. Altermatt and E. A. Fronhofer. “Dispersal in dendritic networks: Ecological consequences on the spatial distribution of population densities”. In: *Freshwater Biology* 63.1 (2018), pp. 22–32. DOI: 10.1111/fwb.12951.
- [64] J. L. Richardson et al. “Microgeographic adaptation and the spatial scale of evolution”. In: *Trends in Ecology & Evolution* 29.3 (2014), pp. 165–176. DOI: 10.1016/j.tree.2014.01.002.
- [65] M. Slatkin. “GENE FLOW AND SELECTION IN A CLINE”. In: *Genetics* 75.4 (1973), pp. 733–756. DOI: 10.1093/genetics/75.4.733.
- [66] M. Kirkpatrick and N. H. Barton. “Evolution of a Species’ Range”. In: *The American Naturalist* 150.1 (1997), pp. 1–23. DOI: 10.1086/286054.
- [67] J. Polechová and N. H. Barton. “Limits to adaptation along environmental gradients”. In: *Proceedings of the National Academy of Sciences of the United States of America* 112.20 (2015), pp. 6401–6406. DOI: 10.1073/pnas.1421515112.
- [68] M. Andrade-Restrepo, N. Champagnat, and R. Ferrière. “Local adaptation, dispersal evolution, and the spatial eco-evolutionary dynamics of invasion”. In: *Ecology Letters* 22.5 (2019). Ed. by V. Calcagno, pp. 767–777. DOI: 10.1111/ele.13234.
- [69] S. Bromberger and other Contributors. “JuliaGraphs/LightGraphs.jl”. In: (2017). DOI: 10.5281/ZENODO.1412141.
- [70] C. Rackauckas and Q. Nie. “DifferentialEquations.jl – a performant and feature-rich ecosystem for solving differential equations in Julia”. In: *Journal of Open Research Software* 5 (2017). DOI: 10.5334/jors.151.

2.A Supplementary Note

2.A.1 Mathematical construction of the model

The model is a measure-valued point process [1], so that individuals are represented as dirac functions $\delta_{x_k^{(i)}}$, where $x_k^{(i)} \in \mathcal{X}$ corresponds to the traits' value of individual k located on vertex v_i . Under this formalism, the population on v_i is represented as a sum of dirac functions $\nu^{(i)} = \sum_k^{N^{(i)}} \delta_{x_k^{(i)}}$, where $N^{(i)}$ is the local population size.

It follows that the time variation of the process can be described by the so-called infinitesimal generator L , defined for all real valued functions ϕ as

$$L\phi(\nu_t^{(i)}) = \partial_t \mathbb{E} [\phi(\nu_t^{(i)})] \quad (\text{S1})$$

(see [2] for an introduction to infinitesimal generators). Equation (S1) provides the expected time variation at time t of e.g. the population size by choosing $\phi(\nu_t^{(i)}) = \int_{\mathcal{X}} \nu_t^{(i)}(dx)$. Recall that we use $b^{(i)}$ to denote the birth rate on vertex v_i , d for the death rate, μ for the mutation probability, m for the migration probability, $\mathcal{M}(x, y) = \frac{1}{\sqrt{2\pi\sigma_\mu^2}} \exp\left(-\frac{\|x-y\|^2}{2\sigma_\mu^2}\right)$ for the mutation kernel, K for the local carrying capacity, $A = (a_{i,j})_{1 \leq i,j \leq M}$ for the adjacency matrix of the graph G , and $D = (d_1, d_2, \dots, d_M)$ for the vector containing the degree of each vertex. In order to explicitly write the generator L , let us recall that five events of different natures can alter the number of individuals with trait x on vertex v_i :

- an individual on v_i with trait x can give birth to an offspring that does not experience mutations nor migration, at rate $(1 - \mu)(1 - m)b^{(i)}(x)$,
- an individual on v_i with trait y can give birth to an offspring with mutated trait x that does not experience migration, at rate $\mu(1 - m)\mathcal{M}(x, y)b^{(i)}(y)$,
- an individual on v_i with trait x can die, at rate $d(N^{(i)}) = \frac{N^{(i)}}{K} = \frac{1}{K} \int_{\mathcal{X}} \nu_t^{(i)}(dx)$,
- an individual on v_j with trait x can give birth to an offspring that does not experience mutations and migrates to v_i , at rate $\frac{a_{i,j}}{d_j}(1 - \mu)m b^{(j)}(x)$,
- an individual on v_j with trait y can give birth to an offspring with mutated trait x that migrates to v_i , at rate $\frac{a_{i,j}}{d_j}\mu m \mathcal{M}(x, y)b^{(j)}(x)$.

Summing over all all individuals and all vertices yields

$$\begin{aligned} L\phi(\nu_t^{(i)}) &= \int_{\mathcal{X}} \left\{ b^{(i)}(\mathbf{x})(1 - \mu)(1 - m)(\phi(\nu_t^{(i)} + \delta_{\mathbf{x}}) - \phi(\nu_t^{(i)})) \right\} \nu_t^{(i)}(d\mathbf{x}) && \text{births w/o mutations, w/o mutations} \\ &+ \int_{\mathcal{X}} \left\{ \mu(1 - m) \int_{\mathcal{X}} b^{(i)}(y)(\phi(\nu_t^{(i)} + \delta_z) - \phi(\nu_t^{(i)})) \mathcal{M}(\mathbf{x}, y) dy \right\} \nu_t^{(i)}(d\mathbf{x}) && \text{births w/ mutations, w/o mutations} \\ &+ \iint_{\mathcal{X}} \left\{ \frac{1}{K}(\phi(\nu_t^{(i)} - \delta_{\mathbf{x}})) - \phi(\nu_t^{(i)}) \right\} \nu_t^{(i)}(dy) \nu_t^{(i)}(dx) \\ &+ \sum_{j \neq i} \frac{a_{i,j}}{d_j} \int_{\mathcal{X}} \mu m \left\{ \int_{\mathcal{X}} b^{(j)}(y)(\phi(\nu^{(j)} + \delta_{\mathbf{x}}) - \phi(\nu^{(j)})) \mathcal{M}(\mathbf{x}, y) dy \right\} \nu_t^{(j)}(d\mathbf{x}) && \text{migrations w/o mutations} \\ &+ \sum_{j \neq i} \frac{a_{i,j}}{d_j} \int_{\mathcal{X}} \left\{ b^{(j)}(\mathbf{x})(1 - \mu)m(\phi(\nu^{(j)} + \delta_{\mathbf{x}}) - \phi(\nu^{(j)})) \right\} \nu_t^{(j)}(d\mathbf{x}). && \text{migrations w/ mutations} \end{aligned} \quad (\text{S2})$$

Taking expectations in Eq. (S2), one can obtain an equation for the mean trajectory of the quantity of interest, $\mathbb{E} [\phi(\nu_t^{(i)})]$. Nonetheless, Eq. (S2) involves an integral

with respect to $\nu_t^{(i)}(dx)\nu_t^{(i)}(dy)$, making it impossible to obtain an explicit solution. It is therefore unclear whether one can gain insight into the stochastic dynamics from Eq. (S2) without simplifying assumptions. We refer to [3] for a detailed discussion on the topic.

2.A.2 Deterministic approximation

One strategy to overcome the difficulties encountered above is to assimilate the process to its mean trajectory, assuming that $\mathbb{E}[\nu_t^{(i)}] \approx \nu_t^{(i)}$ and further approximating $\nu_t^{(i)}$ with a continuous deterministic function $n_t^{(i)}$. Such strategy inherently neglects the stochasticity of the process, which is reasonable provided that a force dampens the stochastic fluctuations of the quantity of interest.

Setting with no selection

Consider a setting with no selection and recall that in this setting where $x \equiv u \in \mathcal{X} = \mathcal{U}$ we define

$$b^{(i)}(x) \equiv b \quad (\text{S3})$$

By applying the strategy mentioned above and choosing $\phi(n_t^{(i)}) = \int_{\mathcal{X}} n_t^{(i)}(x) dx$, Eq. (S2) transforms into the deterministic approximation of the population size dynamics given in the main-text by

$$\partial_t N_t^{(i)} = N_t^{(i)} \left[b(1-m) - \frac{N_t^{(i)}}{K} \right] + mb \sum_{j \neq i} \frac{a_{i,j}}{d_j} N_t^{(j)}. \quad (\text{S4})$$

Competition stabilises the population size dynamics, which behaves deterministically. This is supported by Fig. S10a, which shows how Eq. (S4) accurately describes the population size for varying migration regimes. Nonetheless, stochastic fluctuations drive the dynamics of the neutral trait distribution. Attempting to characterise the neutral trait distribution with the same strategy, this time setting $\phi(n_t^{(i)}) = n_t^{(i)}(u)$, yields

$$\begin{aligned} \partial_t n_t^{(i)}(u) &= n_t^{(i)}(u) \left[b(1-m)(1-\mu) - \frac{1}{K} \int_{\mathcal{U}} n_t^{(i)}(\mathbf{u}) d\mathbf{u} \right] \\ &\quad + (1-m)\mu b \int_{\mathcal{U}} n_t^{(i)}(\mathbf{u}) \mathcal{M}(u, \mathbf{u}) d\mathbf{u} \\ &\quad + m\mu b \sum_{j \neq i} \frac{a_{i,j}}{d_j} \int_{\mathcal{U}} n_t^{(j)}(u) \mathcal{M}(u, \mathbf{u}) d\mathbf{u} \\ &\quad + m(1-\mu)b \sum_{j \neq i} \frac{a_{i,j}}{d_j} b n_t^{(j)}(u). \end{aligned} \quad (\text{S5})$$

Solving for Eq. (S5), one can show that the variance of $n_t^{(i)}$ continuously grows in time (see Fig. S10) and tends to infinity as time goes to infinity, which is an unrealistic behaviour considering finite populations. Intuitively, this reflects the fact that no stabilising force acts on the neutral trait distribution, such that random fluctuations play a major role in driving the dynamics of the stochastic process. Figure S10 shows how IBM trajectories significantly differ from Eq. (S5), and Fig. S11 illustrates how diversity metrics obtained from Eq. (S5) do not match those obtained from simulations of the IBM.

Setting with heterogeneous selection

In contrast to the neutral trait dynamics, the adaptive distribution can successfully be approximated by a deterministic description because selection pressure acts as a stabilising force and stabilises the populations' adaptive trait, dampening the stochastic fluctuations. Consider the setting with heterogeneous selection and recall that in this setting where $x \equiv (s, u) \in \mathcal{X} = \mathcal{S} \times \mathcal{U}$ we define

$$b^{(i)}(x) \equiv b(1 - p(s - \theta_i)^2). \quad (\text{S6})$$

By applying the same strategy as above to characterise the adaptive trait distribution $n_t^{(i)}(s)$ by choosing $\phi(n_t^{(i)}) = n_t^{(i)}(s) \equiv \int_{\mathcal{U}} n_t^{(i)}(u, s) du$, Eq. (S2) transforms into

$$\begin{aligned} \partial_t n_t^{(i)}(s) &= n_t^{(i)}(s) \left[b^{(i)}(s)(1-m)(1-\mu) - \frac{1}{K} \int_{\mathcal{S}} n_t^{(i)}(\mathbf{s}) d\mathbf{s} \right] \\ &\quad + (1-m)\mu \int_{\mathcal{S}} b^{(i)}(\mathbf{s}) n_t^{(i)}(\mathbf{s}) \mathcal{M}(\mathbf{s}, s) d\mathbf{s} \\ &\quad + m\mu \sum_{j \neq i} \frac{a_{i,j}}{d_j} \int_{\mathbb{R}} b^{(j)}(s) n_t^{(j)}(s) \mathcal{M}(\mathbf{s}, s) ds \\ &\quad + m(1-\mu) \sum_{j \neq i} \frac{a_{i,j}}{d_j} b^{(j)}(s) n_t^{(j)}(s). \end{aligned} \quad (\text{S7})$$

Assuming that the variance of the mutation kernel is small, one can use a diffusion approximation for the mutation term [4, 5, 6]

$$\int_{\mathcal{S}} b^{(i)}(\mathbf{s}) n_t^{(i)}(\mathbf{s}) \mathcal{M}(\mathbf{s}, s) d\mathbf{s} = b^{(i)}(s, t) n_t^{(i)}(s) + \frac{1}{2} \sigma_\mu^2 \Delta_s (b^{(i)} n_t^{(i)})(s). \quad (\text{S8})$$

Neglecting the terms in $m\mu$, we obtain

$$\begin{aligned}\partial_t n_t^{(i)}(s) &= n_t^{(i)}(s) \left[b^{(i)}(s, t)(1 - m - \mu) - \frac{1}{K} \int_{\mathcal{S}} n_t^{(i)}(\mathbf{s}) d\mathbf{s} \right] \\ &\quad + \mu \left[b^{(i)}(s, t) n_t^{(i)}(s) + \frac{1}{2} \sigma_\mu^2 \Delta_s (b^{(i)} n_t^{(i)})(s) \right] \\ &\quad + m \sum_{j \neq i} b^{(j)}(s, t) n_t^{(j)}(s) a_{i,j}\end{aligned}\tag{S9}$$

which, after rearranging terms, yields the elegant deterministic approximation of the adaptive trait dynamics

$$\partial_t n_t^{(i)}(s) = n_t^{(i)}(s) \left[b^{(i)}(s)(1 - m) - \frac{1}{K} \int_{\mathcal{S}} n_t^{(i)}(\mathbf{s}) d\mathbf{s} \right] + m \sum_{j \neq i} b^{(j)}(s) \frac{a_{i,j}}{d_j} n_t^{(j)}(s) + \frac{1}{2} \mu \sigma_\mu^2 \Delta_s [b^{(i)}(s) n_t^{(i)}(s)].\tag{S10}$$

Setting $m = 0$ [6] shows that Eq. (S10) admits a stationary solution that is Gaussian, with variance $\sqrt{\mu\sigma_\mu^2}/\sqrt{p}$. Therefore, the variance of the adaptive trait distribution stabilises to a finite value. Intuitively, this reflects the fact that the random fluctuations of the adaptive trait distribution are dampened by the stabilising force of selection. Provided that the selection strength p is large enough, Eq. (S10) is a good approximation of the adaptive trait distribution obtained from the stochastic process. Figure S3 shows how IBM trajectories are similar to the ones obtained from Eq. (S5), and Fig. S4 illustrates how diversity metrics obtained from Eq. (S5) match those obtained from simulations of the IBM.

2.A.3 Trait-dependent competition

To test whether the effects of the metrics hold under more complex ecological processes, we designed an extra experiment considering heterogeneous selection and adaptive trait-dependent competition, where the death rate of individuals on v_i with traits $x_k^{(i)} = (u_k^{(i)}, s_k^{(i)}) \in \mathcal{U} \times \mathcal{S}$ is given by

$$d(x_k^{(i)}, \nu^{(i)}) = \frac{1}{K} \int_{\mathcal{S}} \exp\left(-\frac{(s_k^{(i)} - \mathbf{s})^2}{2\sigma_\alpha^2}\right) \nu^{(i)}(\mathbf{s})\tag{S11}$$

where σ_α is the competition bandwidth. This competition kernel tends to increase the population size, as it decreases the overall competition. The adaptive dynamics theory predicts that when $m = 0$, competition promotes two distinct types of individuals at either side of the adaptive trait optimum for a competition bandwidth $\sigma_\alpha < 1/\sqrt{2p}$, while a single type is observed when $\sigma_\alpha > 1/\sqrt{2p}$ [7]. We performed simulations in both cases for graphs with $M = 7$ vertices and show results of the

multivariate regression analyses in Table S5. The analyses demonstrate that the trends reported in the main manuscript remain unchanged in both cases.

2.A.4 Derivation of the habitat assortativity metric r_Θ in binary environments

We demonstrate here how the habitat assortativity r_Θ relates to the conditional probability of habitats being connected, and we show how r_Θ simplifies under mean field assumption.

Following the original definition of [8], habitat assortativity r_Θ is defined as the Pearson correlation of environmental conditions θ at either ends of the vertices V of graph G , that is

$$r_\Theta = \frac{\text{Cov}(\Theta_x, \Theta_\wedge)}{\sqrt{\text{Var}(\Theta_x)\text{Var}(\Theta_\wedge)}} = \frac{\langle\Theta_x\Theta_\wedge\rangle - \langle\Theta_x\rangle\langle\Theta_\wedge\rangle}{\sqrt{(\langle\Theta_x^2\rangle - \langle\Theta_x\rangle^2)(\langle\Theta_\wedge^2\rangle - \langle\Theta_\wedge\rangle^2)}} \quad (\text{S12})$$

where Θ_x and Θ_\wedge denote the sets of environmental conditions found at the toe and tip of each directed vertex of graph V , and $\langle\Theta_x\rangle$ and $\langle\Theta_\wedge\rangle$ denote their respective mean values.

Let $P(\bullet, \bullet)$ be the proportion of edges that connect a vertex of habitat type \bullet to a vertex of habitat type \bullet . One can also view $P(\bullet, \bullet)$ as the conditional probability that a vertex of type \bullet is connected to a vertex of type \bullet . Let $P(\bullet)$ denote the proportion of vertices that are of type \bullet . First observe that for undirected graphs, one has $\langle\Theta_x\rangle = \langle\Theta_\wedge\rangle$ and $\langle\Theta_x^2\rangle = \langle\Theta_\wedge^2\rangle$. Assuming that habitats are symmetric and binary, it follows that $\theta_\bullet = -\theta_\bullet$. Then

$$\begin{aligned} \langle\Theta_x\Theta_\wedge\rangle &= P(\bullet, \bullet)\theta_\bullet^2 + P(\bullet, \bullet)\theta_\bullet^2 + [P(\bullet, \bullet) + P(\bullet, \bullet)]\theta_\bullet\theta_\bullet \\ &= \theta_\bullet^2 (P(\bullet, \bullet) + P(\bullet, \bullet) - [P(\bullet, \bullet) + P(\bullet, \bullet)]), \end{aligned} \quad (\text{S13})$$

$$\begin{aligned} \langle\Theta_x\rangle &= P(\bullet)\theta_\bullet + P(\bullet)\theta_\bullet \\ &= \theta_\bullet [P(\bullet) - P(\bullet)], \end{aligned} \quad (\text{S14})$$

$$\begin{aligned} \langle\Theta_x^2\rangle &= P(\bullet)\theta_\bullet^2 + P(\bullet)\theta_\bullet^2 \\ &= \theta_\bullet^2 [P(\bullet) + P(\bullet)] \\ &= \theta_\bullet^2. \end{aligned} \quad (\text{S15})$$

Combining Eq. (S13), Eq. (S14) and Eq. (S15) with Eq. (S12) one gets

$$\begin{aligned} r_\Theta &= \frac{\langle \Theta_x \Theta_\wedge \rangle - \langle \Theta_x \rangle \langle \Theta_\wedge \rangle}{\langle \Theta_x^2 \rangle - \langle \Theta_x \rangle^2} \\ &= \frac{P(\bullet, \bullet) + P(\bullet, \bullet) - [P(\bullet, \bullet) + P(\bullet, \bullet)] - (P(\bullet) - P(\bullet))^2}{P(\bullet) + P(\bullet) - (P(\bullet) - P(\bullet))^2} \\ &= \frac{P(\bullet, \bullet) + P(\bullet, \bullet) - [P(\bullet, \bullet) + P(\bullet, \bullet)] - (P(\bullet) - P(\bullet))^2}{1 - (P(\bullet) - P(\bullet))^2}. \end{aligned} \quad (\text{S16})$$

Assuming that habitats are homogeneously distributed, we have $P(\bullet) = P(\bullet) = \frac{1}{2}$ and thus we obtain

$$r_\Theta = P(\bullet, \bullet) + P(\bullet, \bullet) - [P(\bullet, \bullet) + P(\bullet, \bullet)]. \quad (\text{S17})$$

The mean field approximation involves the assumption that all vertices with similar habitats are equivalent in terms of their connections with other habitats, so that $P(\bullet, \bullet) = P(\bullet, \bullet)$ and $P(\bullet, \bullet) = P(\bullet, \bullet)$, which yields $r_\Theta = 2(P(\bullet, \bullet) - P(\bullet, \bullet))$.

References

- [1] V. Bansaye and S. Méléard. “Some stochastic models for structured populations : scaling limits and long time behavior”. In: *Stochastic Models for Structured Populations: Scaling Limits and Long Time Behavior* (2015), pp. 1–107. DOI: 10.1007/978-3-319-21711-6. arXiv: 1506.04165.
- [2] H. Linke. “Applications of Brownian Motion”. In: 5114 (2015), pp. 199–213. DOI: 10.1142/9789814678940_0009.
- [3] N. Champagnat, R. Ferrière, and S. Méléard. “Unifying evolutionary dynamics: From individual stochastic processes to macroscopic models”. In: *Theoretical Population Biology* 69.3 (2006), pp. 297–321. DOI: 10.1016/j.tpb.2005.10.004.
- [4] M. Kimura. “A stochastic model concerning the maintenance of genetic variability in quantitative characters.” In: *Proceedings of the National Academy of Sciences of the United States of America* 54.3 (1965), pp. 731–736. DOI: 10.1073/pnas.54.3.731.
- [5] F. Débarre, O. Ronce, and S. Gandon. “Quantifying the effects of migration and mutation on adaptation and demography in spatially heterogeneous environments”. In: *Journal of Evolutionary Biology* 26.6 (2013), pp. 1185–1202. DOI: 10.1111/jeb.12132.

- [6] S. Mirrahimi and S. Gandon. “Evolution of specialization in heterogeneous environments: equilibrium between selection, mutation and migration”. In: *Genetics* 214.2 (2020), pp. 479–491. DOI: 10.1534/genetics.119.302868.
- [7] M. Doebeli. *Adaptive diversification*. Monographs in population biology. Princeton, N.J: Princeton University Press, 2011.
- [8] M. E. J. Newman. “Mixing patterns in networks”. In: *Physical Review E* 67.2 (2003), p. 026126. DOI: 10.1103/PhysRevE.67.026126. arXiv: 0209450 [cond-mat].
- [9] W.-N. Ding et al. “Ancient orogenic and monsoon-driven assembly of the world’s richest temperate alpine flora”. In: *Science* 369.6503 (2020), pp. 578–581. DOI: 10.1126/science.abb4484.
- [10] M. Jung et al. “A global map of terrestrial habitat types”. In: *Scientific Data* 7.1 (2020), p. 256. DOI: 10.1038/s41597-020-00599-8.
- [11] D. N. Karger et al. “Climatologies at high resolution for the earth’s land surface areas”. In: *Scientific Data* 4.1 (2017), p. 170122. DOI: 10.1038/sdata.2017.122. arXiv: 1607.00217.

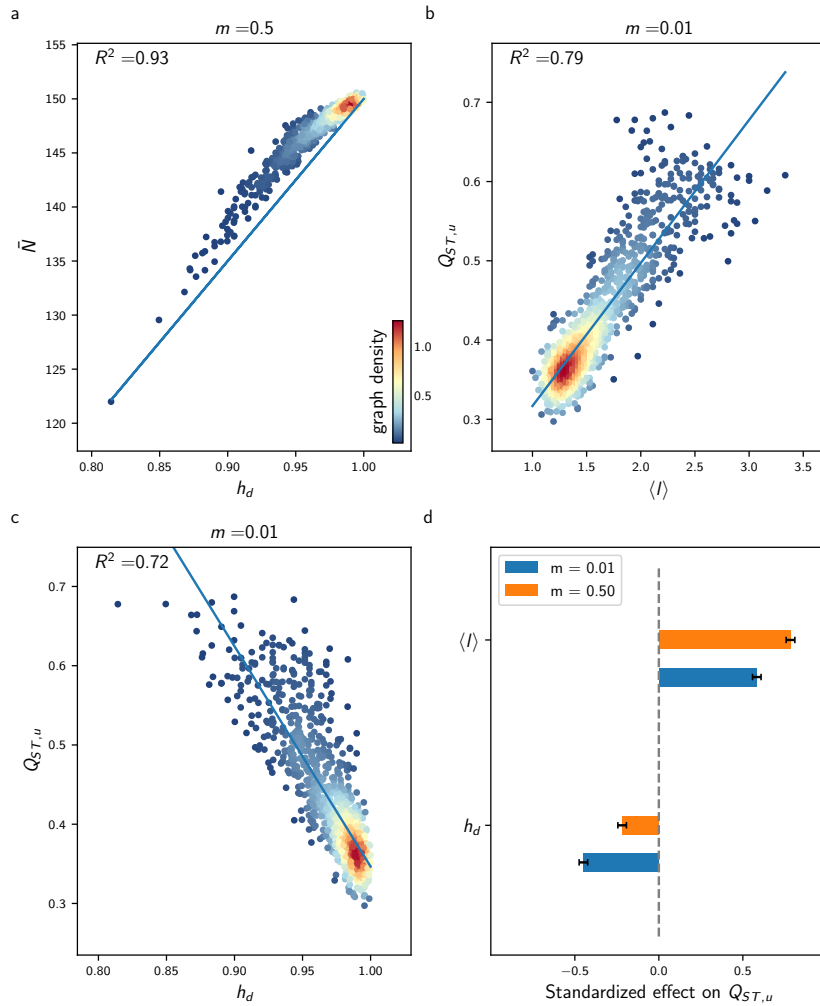


Fig. S1: Effect of $\langle l \rangle$ and h_d on average population size \bar{N} and neutral differentiation $Q_{ST,u}$ under the setting with no selection, analogous to Fig. 2.2 but for 1126 of the 261,080 undirected connected graphs with $M = 9$ vertices.

2.B Supplementary Figures

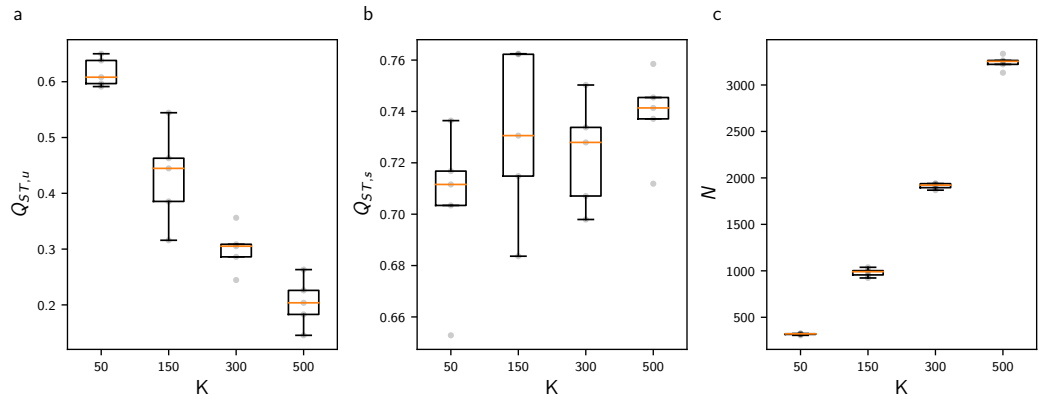


Fig. S2: Effect of the carrying capacity K on $Q_{ST,u}$, $Q_{ST,s}$ and metapopulation size N for the line graph with $M = 7$ vertices for $m = 0.1$. Decreasing K increases $Q_{ST,u}$ as it favours drift, but it does not influence $Q_{ST,s}$. Each boxplot is based on 5 replicate simulations of the IBM, and fade dots represent single values for each replicate.

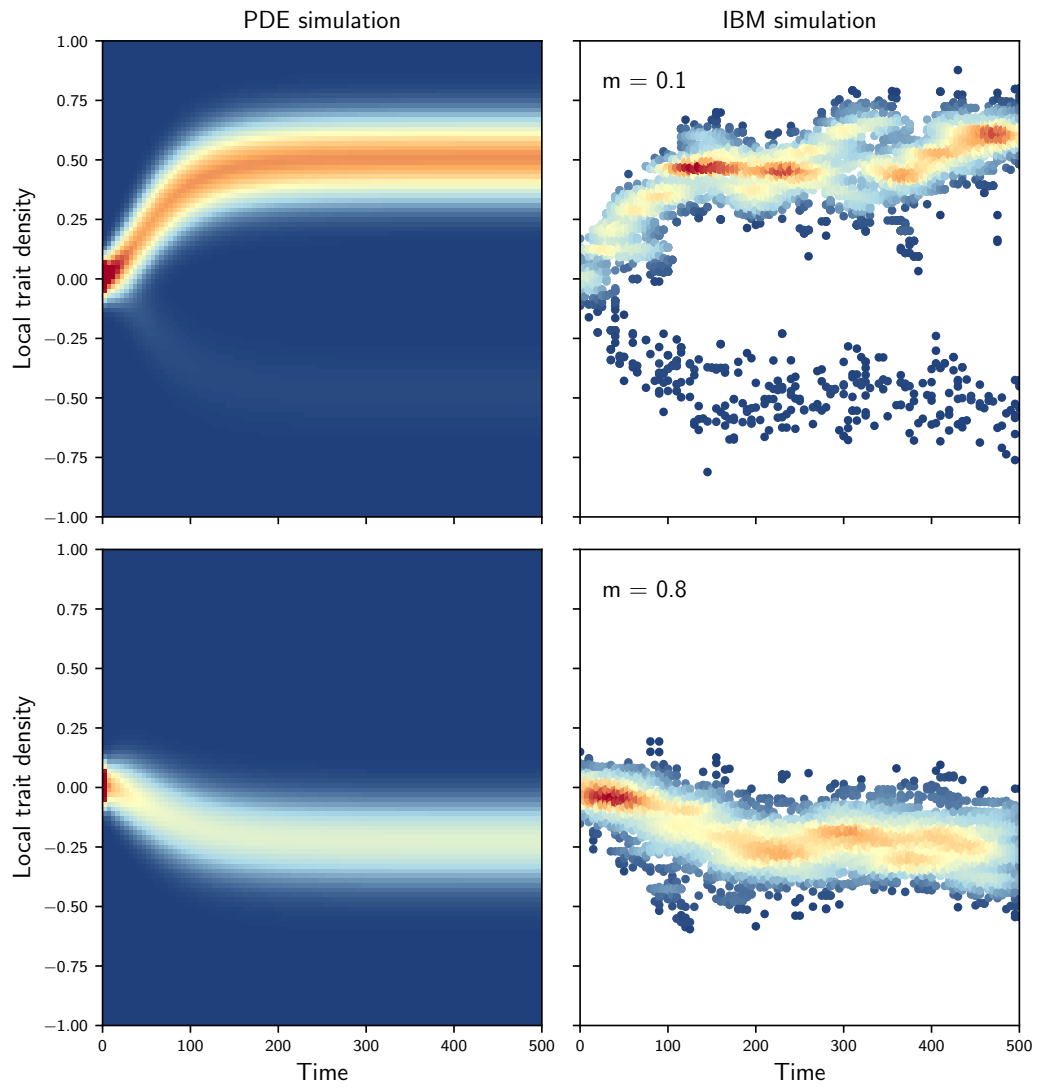


Fig. S3: Comparison of the adaptive trait density on one vertex obtained from Eq. (S10) (left) and from the IBM simulations (right) in the setting with heterogeneous selection, for the star graph with $M = 7$ vertices. The densities obtained from Eq. (S10) and from the IBM are qualitatively similar.

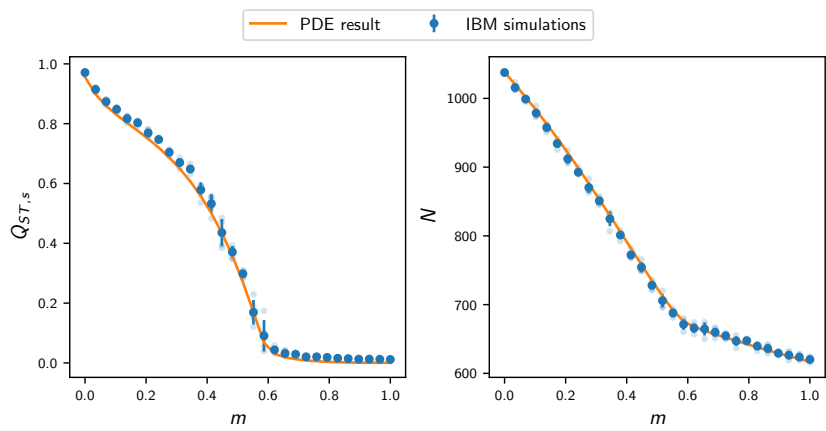


Fig. S4: Comparison of $Q_{ST,s}$ and N obtained from the deterministic approximation Eq. (S10) and from IBM simulations in the setting with heterogeneous selection, on the star graph with $M = 7$ vertices. $Q_{ST,s}$ and population size obtained from Eq. (S10) closely match the IBM simulations. Each plain dot represents average results from 5 replicate simulations of the IBM, bars represent one standard deviation, and each fade dot represents a single replicate value.

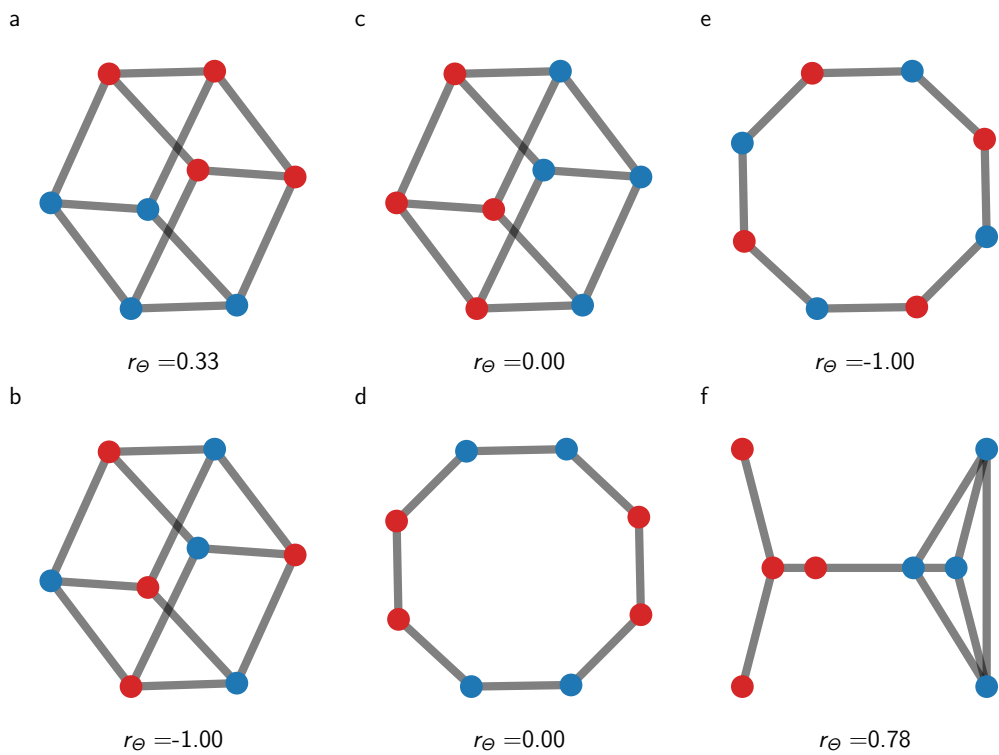


Fig. S5: Graphs with spatial distribution of habitat types corresponding to different habitat assortativity r_Θ . Graphs (a-d) can be described exactly with a mean field approach, as blue and red vertices have an equivalent position on the graph.

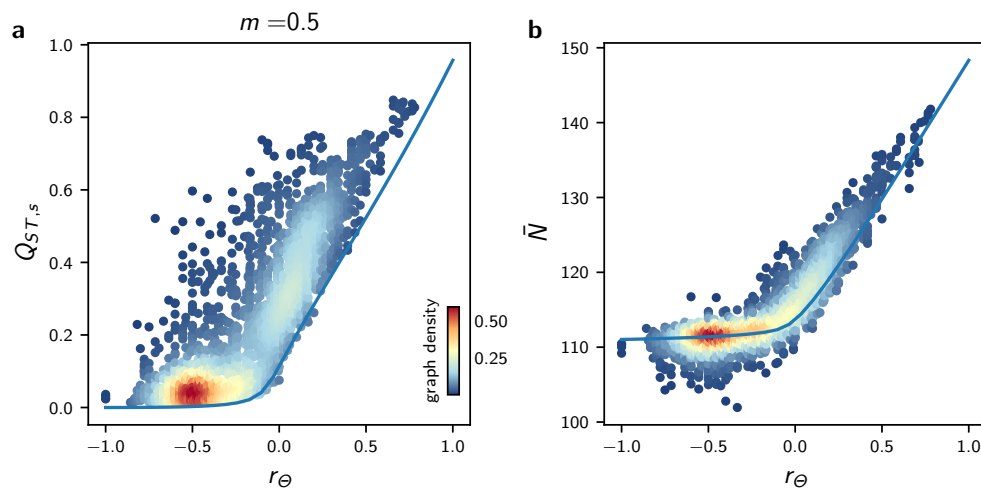


Fig. S6: Effects of habitat heterogeneity r_Θ on $Q_{ST,s}$ and average population size \bar{N} for all undirected connected graphs with $M = 7$ vertices and varying r_Θ , obtained for similar simulations to those in Fig. 2.4 with $m = 0.5$. In (a) and (b), each dot represents average results from 5 replicate simulations of the IBM, the colour scale corresponds to the proportion of the graph with similar x and y axis values (graph density), and the blue lines correspond to results obtained from the mean field, deterministic approximation Eq. (2.5). Deviations from the mean field, deterministic approximation Eq. (2.5) can be explained by differences in $\langle l \rangle$ and h_d between the graphs.

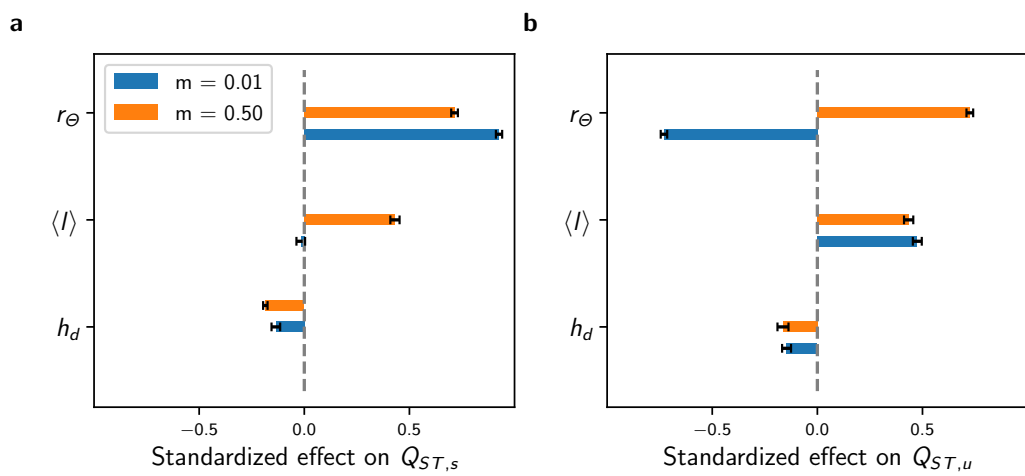


Fig. S7: Standardized effects of h_d , $\langle I \rangle$ and r_Θ on $Q_{ST,s}$ and $Q_{ST,u}$ obtained from multi-variate regression models independently fitted for low and high migration regimes on average results from 5 replicate simulations of the IBM, analogous Fig. 2.5c-d but for 1126 of the 261,080 undirected connected graphs with $M = 9$ vertices and varying r_Θ (see Methods for details). Error bars show 95% confidence intervals.

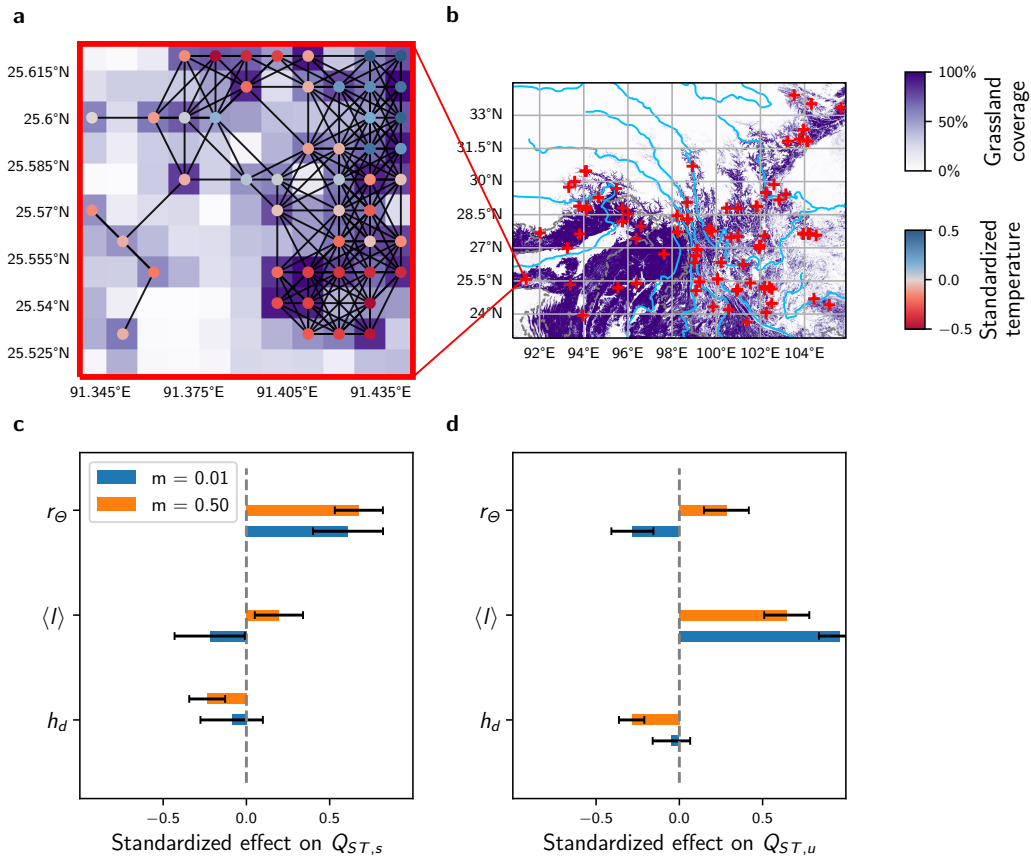


Fig. S8: Simulations on graphs with $M = 49$ vertices obtained from real spatial habitat datasets, in the setting with heterogeneous selection. The region from where graphs are obtained is centred on the Hengduan Mountains in Southwest China, one of the most species-rich temperate mountain biota globally [9]. (a) Graphical representation of a geographical area of size $0.11^\circ \times 0.11^\circ$. To create the graph, we considered biological populations living in grasslands, and used the dataset provided in [10] containing global grassland coverage at 0.01° resolution. We assigned a vertex to a geographical area of size $0.01^\circ \times 0.01^\circ$ if its grassland coverage was above a threshold arbitrarily set to 50%. We further assumed that two vertices were connected if their euclidean distance was below a certain dispersal range, which we let vary from 1 to 2.5 km. Local annual average temperature was considered as the value that captures environmental conditions at each vertex. Temperature data was obtained from the CHELSA dataset [11]. (b) Grassland coverage for the considered region. Blue lines correspond to rivers and dashed grey lines correspond to country borders. Red crosses indicate the locations of the 83 graphs sampled for the simulations used in (c-d). (c-d) Standardized effects of h_d , $\langle l \rangle$ and r_Θ on $Q_{ST,s}$ and $Q_{ST,u}$ obtained from multivariate regression models independently fitted for low and high migration regimes to average results from 5 replicate simulations of the IBM on the 83 graphs which location is illustrated in (c) (see Table S4 for simulation details). Error bars show 95% confidence intervals.

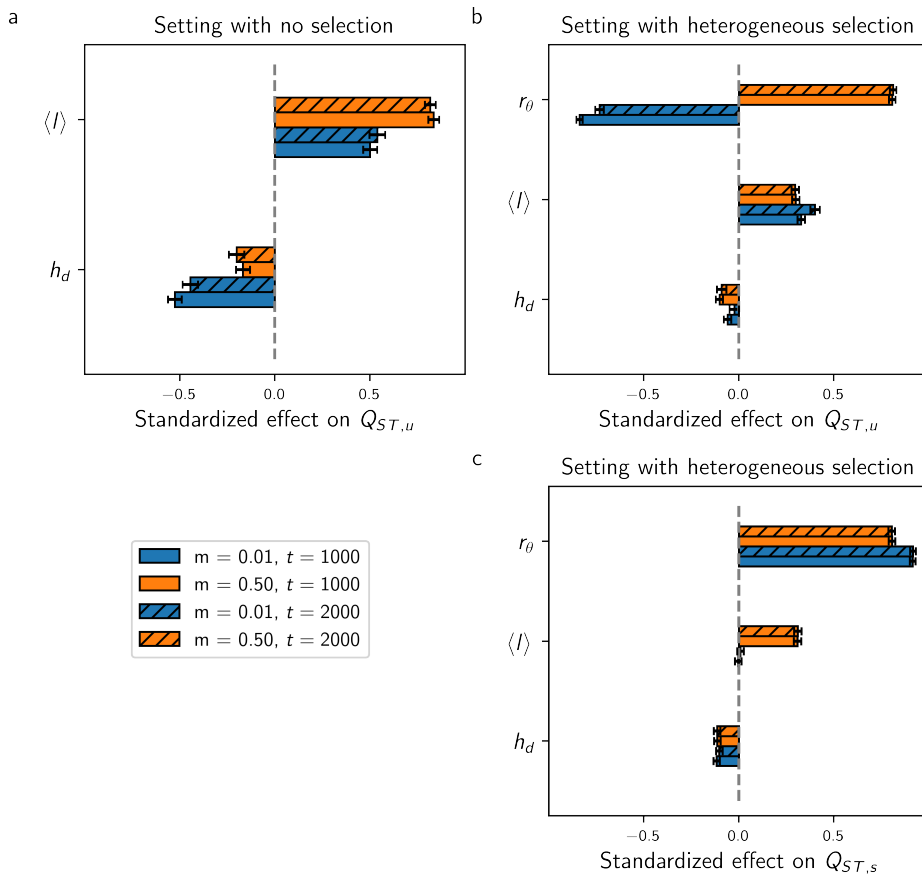


Fig. S9: Standardized effects of h_d , $\langle I \rangle$ and r_θ on $Q_{ST,u}$ in the setting with no selection and in the setting with heterogeneous selection for the time horizons $t = 1000$ and $t = 2000$, obtained from multivariate regression models independently fitted for low and high migration regimes to average results from 5 replicate simulations of the IBM on all undirected connected graphs with $M = 7$ vertices and varying r_θ (see Methods for details). (a–c) illustrate that the effects of the topology metrics on $Q_{ST,u}$ and $Q_{ST,s}$ remain constant for $t > 1000$ in both the settings without selection and with heterogeneous selection. Error bars show 95% confidence intervals.

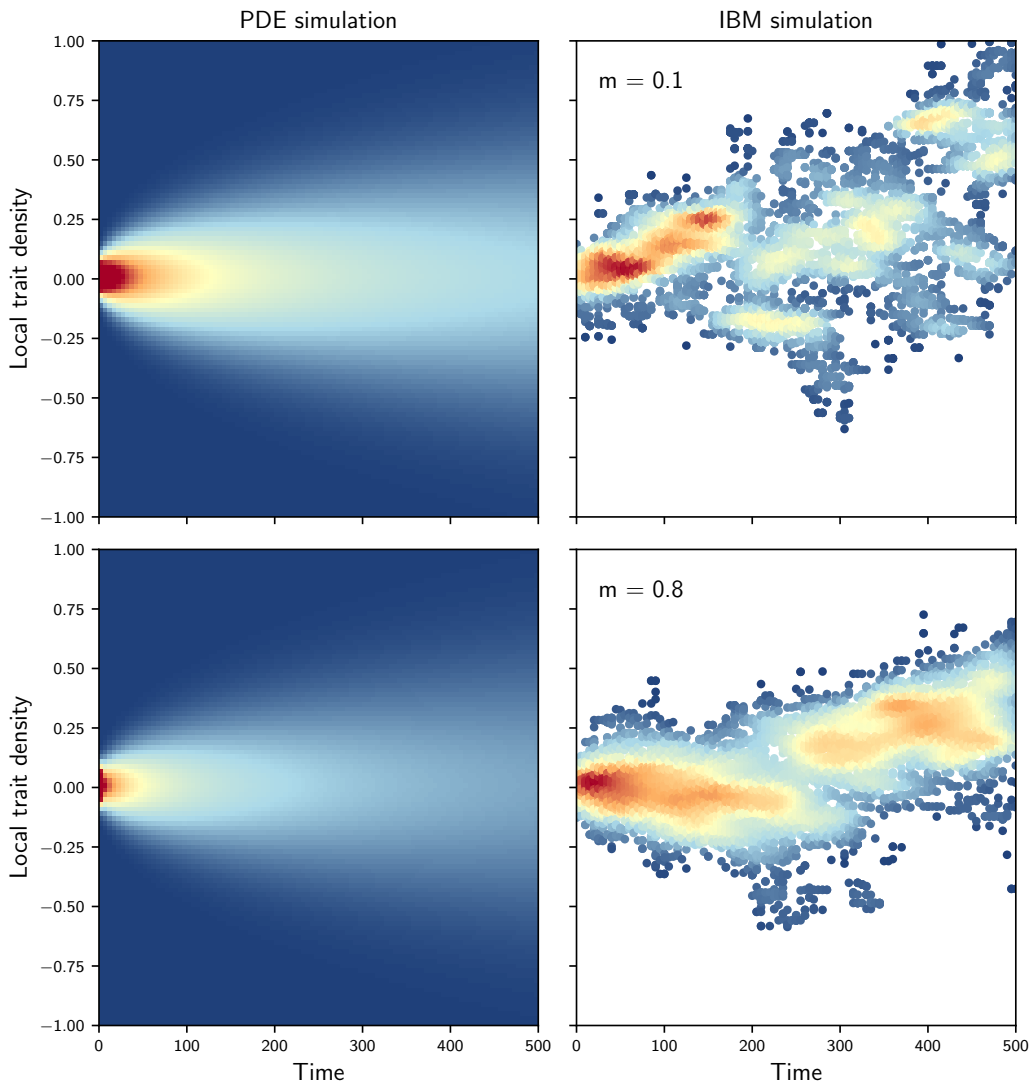


Fig. S10: Comparison of the neutral trait density on one vertex obtained from Eq. (S5) (left) and from the IBM simulations (right) in the setting with no selection, for the chain graph. The densities obtained from Eq. (S5) and from the IBM are dissimilar.

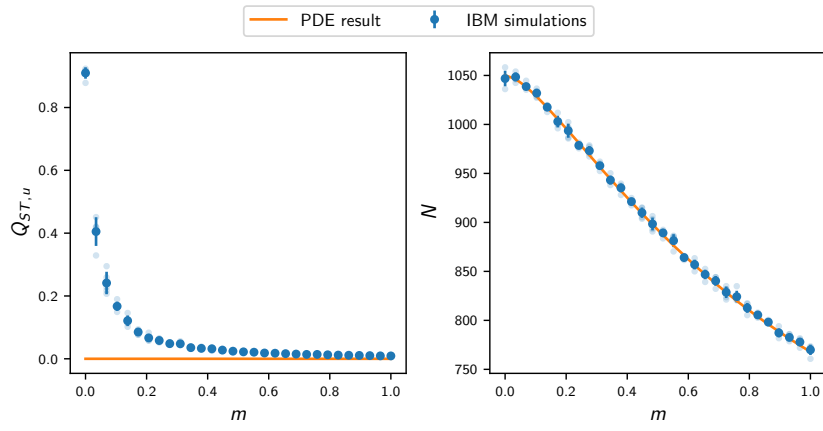


Fig. S11: Comparison of results obtained from the deterministic approximations Eqs. (S4) and (S5) and from IBM simulations in the setting with no selection, on the star graph with $M = 7$ vertices. While Eq. (S4) can capture population size, Eq. (S5) is not able to capture $Q_{ST,u}$. Each plain dot represents average results from 5 replicate simulations, bars represent one standard deviation, and each fade dot represents a single replicate value.

2.C Supplementary Tables

Tab. S1: Linear regression model coefficients for the effect of topology metrics on $Q_{ST,u}$ in the setting with no selection, based on all graphs with $M = 7$ vertices. *** $P < 0.001$

m	$Q_{ST,u}$				$Q_{ST,u} - bN$	
	0.01	0.50	0.01	0.50	0.01	0.50
(Intercept)	0.000 (0.023)	-0.000 (0.017)	-0.000 (0.023)	-0.000 (0.025)	-0.000 (0.023)	-0.000 (0.028)
$\langle l \rangle$	0.739*** (0.023)	0.872*** (0.017)				
h_d			-0.753*** (0.023)	-0.674*** (0.025)	-0.753*** (0.023)	-0.143*** (0.028)
Number of sim.	853	853	853	853	853	853
R^2	0.546	0.760	0.567	0.454	0.567	0.030

Tab. S2: Multivariate linear regression model coefficients for the effect of topology metrics on $Q_{ST,u}$ in the setting with no selection. *** $P < 0.001$

m	$M = 7$				$M = 9$			
	$Q_{ST,u}$							
	0.01	0.50	0.01	0.50				
(Intercept)	-0.000 (0.017)	-0.000 (0.013)	0.000 (0.009)	-0.000 (0.010)				
h_d	-0.527*** (0.019)	-0.352*** (0.014)	-0.449*** (0.013)	-0.218*** (0.013)				
$\langle l \rangle$	0.500*** (0.019)	0.712*** (0.014)	0.583*** (0.013)	0.784*** (0.013)				
Number of sim.	853	853	1,126	1,126				
R^2	0.766	0.858	0.899	0.896				

Tab. S3: Multivariate linear regression model coefficients for the effect of the topology metrics on $Q_{ST,u}$ and $Q_{ST,s}$ in the setting with heterogeneous selection. *** $P < 0.001$

m	$M = 7$				$M = 9$			
	$Q_{ST,s}$		$Q_{ST,u}$		$Q_{ST,s}$		$Q_{ST,u}$	
	0.01	0.50	0.01	0.50	0.01	0.50	0.01	0.50
(Intercept)	-0.000 (0.008)	-0.000 (0.009)	-0.000 (0.009)	-0.000 (0.009)	0.000 (0.008)	0.000 (0.008)	0.000 (0.008)	0.000 (0.008)
h_d	-0.117*** (0.009)	-0.114*** (0.010)	-0.060*** (0.010)	-0.102*** (0.010)	-0.135*** (0.010)	-0.185*** (0.011)	-0.146*** (0.011)	-0.164*** (0.011)
$\langle l \rangle$	-0.004 (0.009)	0.308*** (0.010)	0.328*** (0.010)	0.300*** (0.010)	-0.017 (0.010)	0.431*** (0.011)	0.475*** (0.011)	0.434*** (0.011)
r_Θ	0.914*** (0.008)	0.805*** (0.009)	-0.838*** (0.009)	0.807*** (0.009)	0.926*** (0.008)	0.715*** (0.008)	-0.730*** (0.008)	0.725*** (0.008)
Number of sim.	2,548	2,548	2,548	2,548	2,250	2,250	2,250	2,250
R^2	0.845	0.808	0.808	0.799	0.870	0.853	0.862	0.851

Tab. S4: Multivariate linear regression model coefficients for the effect of topology metrics on $Q_{ST,u}$ and $Q_{ST,s}$ on real graphs with $M = 49$ vertices in the setting with heterogeneous selection. * $P < 0.05$, ** $P < 0.01$, *** $P < 0.001$

m	$Q_{ST,s}$		$Q_{ST,u}$	
	0.1	0.50	0.1	0.50
(Intercept)	-0.000 (0.093)	-0.000 (0.064)	0.000 (0.056)	-0.000 (0.059)
h_d	-0.088 (0.094)	-0.235*** (0.065)	-0.048 (0.057)	-0.286*** (0.060)
$\langle l \rangle$	-0.220* (0.106)	0.195** (0.073)	0.965*** (0.064)	0.645*** (0.068)
r_Θ	0.610*** (0.106)	0.675*** (0.073)	-0.282*** (0.063)	0.282*** (0.068)
Number of sim.	83	83	83	83
R^2	0.313	0.675	0.752	0.717

Tab. S5: Multivariate linear regression model coefficients for the effect of topology metrics on $Q_{ST,u}$ and $Q_{ST,s}$ in the setting of trait-dependent competition and heterogeneous selection (Section 2.A.3), based on all graphs with $M = 7$ vertices. ***
 $P < 0.001$

m	$\sigma_a = 0.5 < 1/\sqrt{2p}$				$\sigma_a = 1 > 1/\sqrt{2p}$			
	$Q_{ST,s}$		$Q_{ST,u}$		$Q_{ST,s}$		$Q_{ST,u}$	
	0.05	0.50	0.05	0.50	0.05	0.50	0.05	0.50
(Intercept)	0.000 (0.005)	-0.000 (0.010)	-0.000 (0.011)	-0.000 (0.010)	0.000 (0.004)	-0.000 (0.008)	0.000 (0.012)	-0.000 (0.007)
h_d	-0.228*** (0.006)	-0.118*** (0.011)	-0.171*** (0.012)	-0.169*** (0.012)	-0.166*** (0.004)	-0.128*** (0.009)	-0.178*** (0.013)	-0.139*** (0.008)
$\langle l \rangle$	0.084*** (0.006)	0.373*** (0.011)	0.461*** (0.012)	0.573*** (0.012)	0.002 (0.004)	0.296*** (0.009)	0.483*** (0.013)	0.286*** (0.008)
r_Θ	0.922*** (0.005)	0.741*** (0.010)	-0.657*** (0.011)	0.508*** (0.010)	0.967*** (0.004)	0.816*** (0.008)	-0.585*** (0.012)	0.837*** (0.007)
Number of sim.	2,548	2,548	2,548	2,548	2,548	2,548	2,548	2,548
R^2	0.934	0.768	0.716	0.732	0.962	0.828	0.659	0.861

Discussion

„ Les données pertinentes détiennent les réponses.

— French anagram

3.1 Contributions

The study of biological and economic systems is a study of the ecological and evolutionary processes, and the resulting mechanisms, that act at different levels of organization and result in cohesive dynamics [1]. Key challenges are to disentangle the necessary and sufficient elemental processes, and understand their couplings.

Addressing those challenges, my work aimed at advancing our quantitative understanding of how ecological and evolutionary processes, and their interplay, shape the dynamics of biological and economic systems. In particular, this thesis contributed to

- (i) a fundamental understanding of the role of eco-evolutionary processes in shaping the dynamics of biological populations structured in complex landscapes [chap1],
- (ii) the quantification of the effect of eco-evolutionary processes in economic systems ??,
- (iii) methodological advances in the forward and inverse modelling of eco-evolutionary dynamics in biological and economic systems ??????.

In the following, I discuss the chapters of my thesis collectively within the broader context of our fundamental understanding and the modelling paradigm of the dynamics of biological and economic systems.

3.1.1 Advances in the fundamental understanding of biological and economic systems

Linking processes to patterns

Spatial patterns of biodiversity result from microscopic processes acting upon individual organisms [2]. Mutations result in the process of genetic drift, which

promotes stochastic variations in the allelic proportions and phenotypes of biological populations [XXX]. In spatially structured populations, this results in turn to "neutral differentiation", where spatially separated populations are inevitably characterised by differentiated alleles and traits [XXX]. The process of dispersal tends to reduce neutral differentiation, and this effect is modulated by landscape connectivity [3, 4, 5] through the mechanism of "isolation by limited dispersal" [6]. By increasing the dispersal ability of organisms, landscape connectivity decreases neutral differentiation. When landscapes present heterogeneous habitats, natural selection can supplement the effect of genetic drift and increase the sole effect of stochasticity on differentiation. Under this scenario, local environment conditions select individuals with traits that provide them higher fitness [XXX]. At the population level, this results in populations adapting to their local environment, a mechanism coined "local adaptation" [7] and resulting in patterns of "adaptive differentiation". Adaptive differentiation is hindered by dispersal, which prevents local adaptation by bringing maladapted individuals, that destabilise the evolution of traits towards the optimal. While adaptive differentiation concerns traits under selection, it indirectly affects the differentiation of neutral traits, that are co-evolving with traits under selection through linkages [XXX]. This results in the mechanism of "isolation by adaptation", where habitat heterogeneity, rather than landscape connectivity, increases neutral differentiation [nosil2008]. Simple mechanisms resulting in neutral and adaptive differentiation are identified, but how they are modulated by eco-evolutionary feedbacks and landscape complexity is unclear.

In ??, I demonstrate a novel mechanism, involving the ecological process of competition for resources, that considerably affects neutral differentiation. Through the creation of unbalanced migration fluxes which affect the intensity of competition, heterogeneity in connectivity reduces gene flow and reinforces neutral differentiation. Through the accumulation of incompatibilities over time [Dobhsanski], this mechanism could lead to speciation over time, and contribute to the high diversification in mountain regions [Rahbek].

I also investigate the mechanism of local adaptation and how it results in adaptive differentiation in complex landscapes, where habitats are arranged in a realistic fashion. My results show that the complexity of habitat spatial distribution can be reduced to a measure of habitat spatial auto-correlation coined the "habitat assortativity" and denoted by r_Θ . Landscapes characterised by a high r_Θ systematically support populations that are locally better adapted than in landscape with low r_Θ , resulting in higher adaptive differentiation. Specifically, I provide an analytical condition for local adaptation that sheds light on how it relates to dispersal intensity, selection strength, habitat heterogeneity, and r_Θ .

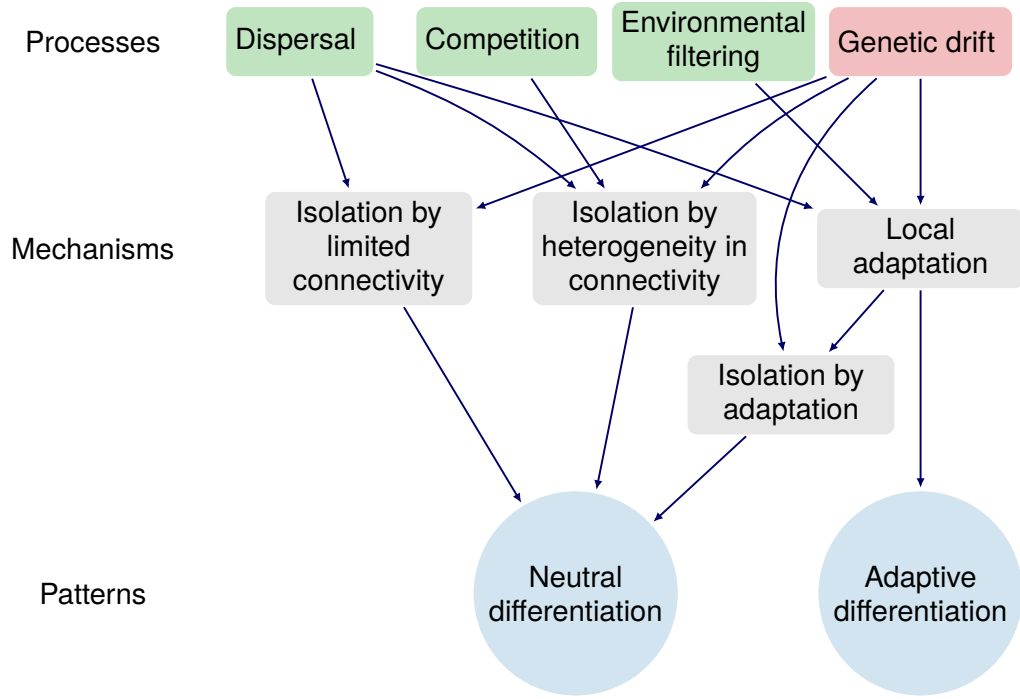


Fig. 3.1: Summary of the causal pathways involved in neutral and adaptive differentiation.

Because r_Θ affects local adaptation, it must affect neutral differentiation through the mechanism of isolation by adaptation. Closing the loop, I demonstrate that r_Θ affects population differentiation through two antagonistic effects. By favoring local adaptation, it promotes isolation by adaptation, therefore increasing neutral differentiation. Nonetheless, it also favors gene flow within clusters of similar environmental conditions, decreasing isolation by limited dispersal. This complex feedback is essential to understand population differentiation in complex landscapes.

Overall, ??links fundamental mechanisms involved in the phenotypic differentiation of populations to eco-evolutionary feedbacks and complex population structures.

Linking patterns to processes

The processes that determine the dynamics of economic systems are unclear. Exogenous drivers, such as technological change [XXX], economic institutions [XXX], and production costs [Boschma2005a] have been proposed, but

References

- [1] S. A. Levin. “Complex adaptive systems: Exploring the known, the unknown and the unknowable”. In: *Bulletin of the American Mathematical Society* 40.01 (2002), pp. 3–20. DOI: 10.1090/S0273-0979-02-00965-5.
- [2] N. Champagnat, R. Ferrière, and S. Méléard. “Unifying evolutionary dynamics: From individual stochastic processes to macroscopic models”. In: *Theoretical Population Biology* 69.3 (2006), pp. 297–321. DOI: 10.1016/j.tpb.2005.10.004.
- [3] S. Wright. “Isolation By Distance”. In: *Genetics* (1943).
- [4] B. H. McRae. “ISOLATION BY RESISTANCE”. In: *Evolution* 60.8 (2006), p. 1551. DOI: 10.1554/05-321.1.
- [5] B. H. McRae and P. Beier. “Circuit theory predicts gene flow in plant and animal populations”. In: *Proceedings of the National Academy of Sciences* 104.50 (2007), pp. 19885–19890. DOI: 10.1073/pnas.0706568104.
- [6] L. Orsini et al. “Drivers of population genetic differentiation in the wild: Isolation by dispersal limitation, isolation by adaptation and isolation by colonization”. In: *Molecular Ecology* 22.24 (2013), pp. 5983–5999. DOI: 10.1111/mec.12561.
- [7] T. J. Kawecki and D. Ebert. “Conceptual issues in local adaptation”. In: *Ecology Letters* 7.12 (2004), pp. 1225–1241. DOI: 10.1111/j.1461-0248.2004.00684.x.

